R. & M. No. 3402

MINISTRY OF AVIATION

AERONAUTICAL RESEARCH COUNCIL
REPORTS AND MEMORANDA

The Calculation of Lateral Stability Derivatives of Slender Wings at Incidence, Including Fin Effectiveness, and Correlation with Experiment

By A. JEAN ROSS, Ph.D.

LONDON: HER MAJESTY'S STATIONERY OFFICE
1965
PRICE 15*s.* 0*d.* NET

The Calculation of Lateral Stability Derivatives of Slender Wings at Incidence, Including Fin Effectiveness, and Correlation with Experiment

By A. Jean Ross, Ph.D.

Communicated by the Deputy Controller Aircraft (Research and Development), Ministry of Aviation

*Reports and Memoranda No. 3402**

March, 1961

Summary.

Comparisons are made between low-speed experimental results and estimates based on attached-flow theory for the lateral stability derivatives of slender wings at incidence, and it is found that the flow separation has little effect on the sideslip derivatives. The reduction in l_v due to part-span anhedral is evaluated, and a semi-empirical formula is derived to account for important second-order terms. For the rotary derivatives, an attempt is made to estimate the effect of the leading-edge vortices, but no satisfactory conclusions have been reached.

The fin contributions to the derivatives are evaluated on the basis of treating the wing surface as a total reflection plate. Good agreement with experiment is reached for the sideslip derivatives, and for the damping-in-yaw at moderate incidences. Sidewash is found to have a large effect on the rolling derivatives, and further information on the strength and position of the leading-edge vortices in non-symmetric flow is required before a complete calculation of the sidewash can be given.

LIST OF CONTENTS

* Replaces R.A.E. Report No. Aero. 2647—A.R.C. 23 089.

LIST OF APPENDICES

LIST OF ILLUSTRATIONS

Figure

1. *Introduction.*

At the present time, a fairly extensive wind-tunnel programme is giving experimental results for the lateral stability derivatives at subsonic speeds of slender wings, of various planforms, span-length ratios, etc. The theoretical calculation of the derivatives has already been given for delta wings with attached flow*, independent of Mach number, in Ref. 1, and the theory is easily extended to other slender planforms. The present report compares the experimental results with those of the attached-flow theory, in order to discover its limitations in subsonic flow, and attempts to calculate the effect of the leading-edge vortices which arise from flow separation when slender wings are at incidence.

The sideslip derivatives are found to be little affected by the leading-edge vortices, and the attached-flow theory is extended so that the reduction in the magnitude of l_v due to putting anhedral on the wing in various ways may be calculated. A semi-empirical formula is then derived for delta wings with drooped tips, which includes second-order terms in angles of incidence and andedral. The leading-edge vortices seem to have an appreciable effect on the derivatives due to rolling, and in fact the attached-flow theory predicts a much greater loss in damping-in-roll with increasing incidence (and the wing rolling about the wind axis), than is found experimentally. Also, the n_p derived in Ref. 1 arises from the suction forces along the leading edge, which vanish when the flow separates, so that a better estimate for n_p, when there is no dihedral, is zero with respect to body axes (i.e. $-l_p\alpha$ for wind-body axes†), which agrees quite well with experiment. The effect of the vortices on the antisymmetric pressure distribution on the rolling wing is calculated from the boundary condition on the wing, in terms of the symmetric loading which can then be taken from theory or experiment. However, this does not lead to a great improvement in the estimation of l_p, and any future theoretical considerations will have to make allowance for the asymmetric strength and position of the vortices from a rolling wing. For the wing alone, the experimental results for derivatives due to yawing are very sparse, and the American oscillatory tests available give results which vary greatly with frequency, so that comparisons with theory are inconclusive. The attached-flow theory of Ribner neglects terms of order A in comparison with those of order $1/A$, and so the result for wings of aspect ratio of order 1 is derived, and a parallel calculation to that for the damping-in-roll is given for the effect of the vortices on the asymmetric pressure distribution. The resulting l_r is found to differ little from the attached-flow result, and the n_r is small for moderate incidences.

The fins of current designs are of relatively simple planforms, and the estimation of their effectiveness is made easier than for the fin and tailplane configuration when the fin is placed on the wing surface. From structural reasons, it is highly probable that the major part of the fin area will lie ahead of the wing trailing edge, and so we may consider the wing surface as a total reflection plate for the net fin. Thus sideslip is equivalent to incidence, yawing to pitching, and rolling to a symmetric distribution of incidence varying linearly along the semispan of the fin. Theoretical estimates for lift and moment due to incidence are available for most planforms, and results for the fin contribution to the sideslip derivatives are in good agreement with experiment. For the rolling motion, a lifting-surface theory has to be used for calculating the lift and moments, and the contri-

* i.e. it is assumed that the flow remains attached throughout the incidence range.

† In order to be concise, the wind-body system of axes will be referred to as wind axes in the remainder of this report.

bution to the l_p and n_p from this effective incidence on the fin is found to be very different from the experimental results. This is due to the sidewash on the fin, which arises from the asymmetric lift distribution on the wing, and the asymmetry in the strength and position of the leading-edge vortices. Attached-flow theory is used to estimate part of the sidewash, but as the incidence of the wing increases the influence of the vortices becomes more important, as is expected, and so more theoretical work will have to be done before satisfactory agreement with experiment is reached. The oscillatory damping-in-yaw, evaluated from the oscillatory damping-in-pitch of the reflected fin, is in satisfactory agreement with experiment up to about 15°, but overestimates the damping at higher incidences.

2. *The Derivatives Due to Sideslip.*

2.1. *Flat-Plate Wings with Full-Span Dihedral.*

Theoretical estimates of the sideslip derivatives y_v, l_v and n_v for low-aspect-ratio delta wings with attached flow are given in Ref. 1, and for slender bodies of general cross-section in Ref. 2. For thin delta wings the results of Ref. 1, referred to wind axes, are

$$\left.\begin{aligned} y_v &= 0 \\ l_v &= -\frac{\pi\alpha}{3} - \frac{A\Gamma}{6} \\ n_v &= \left(\frac{\pi\alpha}{3} + \frac{A\Gamma}{6}\right)\alpha \end{aligned}\right\} \tag{1}$$

where Γ is the dihedral angle, and all the derivatives are independent of the chordwise position of the reference point*.

The analysis may be extended to gothic wings to give

$$\left.\begin{aligned} y_v &= 0 \\ l_v &= -\frac{2\pi\alpha}{5} - \frac{A\Gamma}{6} \\ n_v &= \left(\frac{2\pi\alpha}{5} + \frac{A\Gamma}{6}\right)\alpha. \end{aligned}\right\} \tag{2}$$

These formulae might be expected to hold for small α only, since leading-edge separation effects are neglected, but the results shown in Fig. 1, where experiment[3, 4] and theory are compared for several wings, indicate that, for delta wings of aspect ratio 1, the theory applies satisfactorily up to incidences of 15°. The American tests[3] (Fig. 1a) have also included delta wings of very low aspect ratio, 0·53 and 0·25, for which the y_v and n_v become very erratic as the incidence increases, and l_v shows some slight non-linearities with α. These effects may be due to the leading-edge vortices, but an attempt to calculate l_v led to unsatisfactory answers. For the gothic wing of aspect ratio 1·0 the difference in the slope of the $l_v - \alpha$ curve may be due in part to the 'non-slenderness' of such a planform, where $b/c_0 = 2/3$.

* The term $\pi\alpha^2/3$, which arises from the transformation to wind axes (*see* Appendix I) as $\pi\alpha \sin\alpha/3$, is retained here, although Ribner neglected it. This has been done throughout the report, so that it is possible to account for this part of second-order terms in α, and then any further second-order effects of α shown in the comparison with the experimental results must arise from the leading-edge vortices.

There are also some experimental results[6] for a delta wing of aspect ratio 1·0 with anhedral, and these are compared with the theoretical estimates in Fig. 2. Again the agreement for l_v and n_v is surprisingly good, even for incidences of 15° with anhedral angle of 20°.

Thus we are justified in assuming that the leading-edge vortices do not affect the sideslip derivatives greatly, for wings of aspect ratio of order 1, and so attached-flow theory may be used to estimate effects of thickness, part-span dihedral etc.

2.2. *Wings with Thickness.*

Experimental results reported in Ref. 4 indicate that wing thickness can have an appreciable effect on n_v, and to a smaller extent on l_v. Theoretical estimates can be obtained for wings with spanwise cross-sections which are transformable to a circle, from the formulae given in Ref. 2. The majority of wind-tunnel tests to date have been for wings with diamond cross-sections, for which Maskell has derived the transformation, in some unpublished work. Consider a spanwise cross-section, in the ζ-plane, distance x from the wing apex, of semispan s, and semi-thickness h. In order to use Sacks' formulae[2] we need to transform this to a circle of radius r_0, in the σ-plane, as shown in Fig. 3. The relationship between the two planes is given by

$$\frac{d\zeta}{d\sigma} = \left(\frac{\sigma^2 + {r_0}^2}{\sigma^2 - {r_0}^2}\right)^{2\tau/\pi} \left(1 - \frac{{r_0}^2}{\sigma^2}\right) \tag{3}$$

where

$$\tan \tau = \frac{h}{s}. \tag{4}$$

By integrating along one side AB of the diamond, i.e. along one quadrant A'B' of the circle (*see* Fig. 3), we find that

$$r_0 = s \frac{\pi^{1/2}}{2} \frac{\sec \tau}{\Gamma(1-\tau/\pi)\,\Gamma(\tfrac{1}{2}+\tau/\pi)}. \tag{5}$$

Equations (3) and (5) are sufficient for the evaluation of the sideslip derivatives, and those affected by thickness are given by

$$\frac{dl_v}{d\alpha} = -8\pi A \left(\frac{c_0}{b}\right)^3 \int_0^1 \left(\frac{r_0}{c_0}\right)^2 \left(1 - \frac{4\tau}{\pi}\right) d\left(\frac{x}{c_0}\right) \tag{6}$$

$$n_{v0} = 4A \left(\frac{c_0}{b}\right)^3 \int_0^1 \left\{\left(\frac{s}{c_0}\right)^2 \tan \tau - 4\left(\frac{r_0}{c_0}\right)^2 \tau\right\} d\left(\frac{x}{c_0}\right). \tag{7}$$

The variation of s with x is determined from the planform:

$$\left.\begin{aligned} \frac{s}{c_0} &= \frac{A}{4}\left(\frac{x}{c_0}\right) && \text{for a delta wing} \\ \frac{s}{c_0} &= \frac{A}{3}\left(\frac{x}{c_0}\right)\left(2 - \frac{x}{c_0}\right) && \text{for a gothic wing} \end{aligned}\right\} \tag{8}$$

and the variation of h with x is given by the chordwise thickness distribution, i.e. for the wings under consideration

$$\frac{h}{c_0} = 2\left(\frac{t}{c_0}\right)\left(\frac{x}{c_0}\right)\left(1 - \frac{x}{c_0}\right). \tag{9}$$

The integrals in equations (6) and (7) have to be evaluated numerically, and the results for six different wings are shown in Fig. 4. The experimental results were taken from various sources,

Refs. 4, 5 and 6, in order to cover a large range of thickness/chord ratios. For the delta wings, the estimation of l_v is very good, but for the gothic wings the same order of difference in the slope of the $l_v - \alpha$ curve is observed as in the flat-plate results. The value of n_v at $\alpha = 0$ is slightly overestimated for the thick wings ($t/c = 12\%$), but is in good agreement for the thinner wings, and the variation of n_v with incidence is satisfactorily predicted for all wings.

2.3. *Wings with Part-Span Dihedral.*

Ribner[1] has considered wings with full-span dihedral and his theory is easily extended to account for varying dihedral across the span, for example wings with drooped leading edges.

Consider the wing section where the semispan is s, and let the dihedral-anhedral distribution across the span be that shown in Fig. 3b. The corresponding downwash distribution across the span is given by

$$\left.\begin{aligned} -s < y < -\lambda s, \quad & \frac{w}{V} = \alpha + \gamma_2\beta \\ -\lambda s < y < 0, \quad & \frac{w}{V} = \alpha - \Gamma_2\beta \\ 0 < y < \lambda s, \quad & \frac{w}{V} = \alpha + \Gamma_1\beta \\ \lambda s < y < s, \quad & \frac{w}{V} = \alpha - \gamma_1\beta \end{aligned}\right\} \tag{10}$$

to the first order in α, β and dihedral angles. Following Ribner's analysis[1], the downwash distribution is written as a Fourier cosine series, where $y = s\cos\theta$, and

$$\frac{w}{V} = -A_0 + \sum_1^\infty A_n \cos n\theta . \tag{11}$$

The velocity potential is then given by

$$\begin{aligned} \phi &= Vs\left[-A_0\sin\theta + \frac{A_1}{4}\sin 2\theta + \sum_2^\infty \frac{A_n}{2}\left\{\frac{\sin(n+1)\theta}{n+1} - \frac{\sin(n-1)\theta}{n-1}\right\}\right] \\ &= Vs\sum_1^\infty B_n \sin n\theta, \text{ say}. \end{aligned} \tag{12}$$

For a wing in sideslip, the pressure difference is given by the approximate relation,

$$\Delta p = 2\rho V\left(\frac{\partial\phi}{\partial x} - \beta\frac{\partial\phi}{\partial y}\right)$$

and so the rolling moment, L, is given by

$$\begin{aligned} L &= -\iint \Delta p\, y\, dy\, dx \\ &= -2\rho V\int_{-b/2}^{+b/2}[\phi]_{TE}\, y\, dy + 2\rho V\beta\int_0^c\int_{-s}^{+s}\frac{\partial\phi}{\partial y}\, y\, dy\, dx \\ &= -\rho V^2\left\{\left(\frac{b}{2}\right)^3\frac{\pi}{2}[B_2]_{TE} + \beta\pi B_1\int_0^c s^2 dx\right\}. \end{aligned} \tag{13}$$

From equation (12), we have that

$$\left.\begin{aligned} B_1 &= -A_0 - \frac{A_2}{2} \\ B_2 &= \frac{A_1}{4} - \frac{A_3}{4}, \end{aligned}\right\} \tag{14}$$

and from equations (10) and (11),

$$\left.\begin{aligned} A_0 &= -\alpha + \mathrm{O}(\beta) \\ A_1 &= \frac{2\beta}{\pi}\left[\Gamma_1 + \Gamma_2 - (1-\lambda^2)^{1/2}(\gamma_1+\gamma_2+\Gamma_1+\Gamma_2)\right] \\ A_2 &= \mathrm{O}(\beta) \\ A_3 &= \frac{2\beta}{3\pi}\left[-\Gamma_1 - \Gamma_2 - (1-\lambda^2)^{1/2}(4\lambda^2-1)(\gamma_1+\gamma_2+\Gamma_1+\Gamma_2)\right]. \end{aligned}\right\} \tag{15}$$

Finally, from equations (13), (14) and (15), the result for a delta wing is

$$\begin{aligned} l_v &= \frac{1}{\frac{1}{2}\rho V^2 S b}\frac{dL}{d\beta} \\ &= -\frac{A}{12}\left[\Gamma_1 + \Gamma_2 - (1-\lambda^2)^{3/2}(\gamma_1+\gamma_2+\Gamma_1+\Gamma_2)\right] - \frac{\pi\alpha}{3}. \end{aligned} \tag{16}$$

For a symmetric distribution of dihedral, i.e. $\gamma_1 = \gamma_2 = \gamma$, and $\Gamma_1 = \Gamma_2 = \Gamma$,

$$l_v = -\frac{A}{6}\left[\Gamma - (1-\lambda^2)^{3/2}(\gamma+\Gamma)\right] - \frac{\pi\alpha}{3}. \tag{16a}$$

It is seen from equations (13), (14) and (15) that the dihedral contribution to l_v is independent of the planform of the wing, and so for a gothic wing we have

$$l_v = -\frac{A}{6}\left[\Gamma - (1-\lambda_{\mathrm{TE}}{}^2)^{3/2}(\gamma+\Gamma)\right] - \frac{2\pi\alpha}{5}. \tag{16b}$$

These equations (16), (16a) and (16b) are only strictly true for small dihedral angles, and so the special case of leading edges deflected through 90° was also considered. The cross-section was transformed to a circle, so that the formulae given in Ref. 2 could be used. The transformations necessary are outlined in Appendix II. The numerical work involved is lengthy, since l_v is given as the sum of an infinite series, which was found to converge rather slowly, and only one result, for $\lambda = 3/4$, was obtained.

The only published experimental results[25] available are for a delta wing of aspect ratio 1·56 (with leading-edge sweptback 68·7°), mounted on a body whose maximum diameter is 1/6 of the maximum span of the wing. The wing was hinged at its root chords, and along a line sweptback 77°, so that the outer portion of the wings could be drooped with $\lambda_{\mathrm{TE}} = 0{\cdot}667$. The experimental results are shown in Fig. 5, with the theoretical results. When the dihedral is constant across the semispan (i.e. $\Gamma_1 = -\gamma$), the agreement between experiment and theory for the dihedral contribution to l_v is good for $\Gamma < 20°$, but the slope of the $l_v - \alpha$ curves is overestimated by theory, which may be due partly to the presence of the body, and partly to the comparatively large aspect ratio of

the wing. Drooping the outer portion of the wings by 20° causes a change in the slope of the $l_v - \alpha$ curve at small incidences, which is not indicated by the theory, and the dihedral contribution is overestimated, this being probably due to the large angles involved.

A wing of aspect ratio 1·0, with 25% of the semispan drooped at the leading edges has been tested at the Royal Aircraft Establishment by Kirby, and the unpublished results are compared with theory in Fig. 6. The result from equation (16a), at $\alpha = 0°$, underestimates the effect of the anhedral, as shown in Fig. 5b, for which no satisfactory explanation has been found. It may also be seen from Fig. 5b that the theoretical value for l_v due to deflecting the leading edges through 90° is equal to that due to deflecting them through 30°, so that the linear equation (16) is only valid for small angles of deflection. An empirical relation for large angles of deflection is derived in the following section, and discussion of these results will be given there.

2.4. *Wings with Drooped Tips.*

The analysis for the contribution of drooped tips to l_v is exactly similar to that for part-span dihedral, and the rolling moment is given by equation (14). The Fourier coefficient B_2 is now a function of x, since λ varies with x, and so we have that

$$L = -\rho V^2 \left[\left(\frac{b}{2}\right)^3 \frac{\pi}{2} [B_2]_{\mathrm{TE}} + \beta\pi B_1 \int_0^c s^2 dx \right].$$

To the first order in Γ and γ, s^2 remains unchanged with dihedral, and so for a delta wing with tips drooped through an angle γ, and inboard dihedral Γ,

$$l_v = -\frac{A}{6}[\Gamma - (1-\lambda_{\mathrm{TE}}{}^2)^{3/2}(\gamma+\Gamma)] - \frac{\pi\alpha}{3}. \tag{17}$$

The experimental results from Ref. 6 on a delta wing of aspect ratio 1·0, for two sizes of tips, and three droop angles, are shown in Fig. 7, together with the theoretical results. A comparison indicates that there is an effect of γ on $dl_v/d\alpha$ which has not been accounted for in the first-order theory, and so an analysis of the experimental results was made for the contribution of l_v due to drooped tips at $\alpha = 0°$, and $\alpha = 15°$ with $\Gamma = 0°$, by writing

$$\frac{\Delta l_v}{A(1-\lambda_{\mathrm{TE}}{}^2)^{3/2}} = \frac{\gamma}{6}(1+E\gamma) + F\gamma\alpha.$$

The results are shown in Fig. 9, together with the curves obtained by taking $E = -\frac{1}{2}$, $F = 1$, which are satisfactory mean curves for the experimental points. Thus the empirical formula suggested is

$$l_v = \frac{A}{6}(1-\lambda_{\mathrm{TE}}{}^2)^{3/2}\gamma\left(1-\frac{\gamma}{2}\right) - \alpha\left[\frac{\pi}{3} - A(1-\lambda_{\mathrm{TE}}{}^2)^{3/2}|\gamma|\right]. \tag{18}$$

The modulus of γ is used for the incidence variation, since the experimental results for $\gamma = -20°$ and $-45°$ shown in Fig. 6a indicate a decrease in the magnitude of $dl_v/d\alpha$.

The values for l_v given by equation (18) are shown by the chain-dotted lines in Figs. 6 and 7, and also for the ogee wing with drooped tips in Fig. 8. For this wing[8], l_v is non-linear with α, so that for $\alpha > 5°$, the empirical value of l_v departs from experiment, until at $\alpha = 15°$ the experiment gives only a third of the estimated value. It does not seem possible to predict such non-linearities at present.

3. *The Derivatives Due to Rolling.*

The theory for attached flow[1] gives the damping-in-roll, referred to body axes, as

$$l_{p0} = -\frac{\pi A}{32},$$

for any slender planform, since the rolling moment depends only on the loading at the trailing edge, and not on the chordwise distribution. Both side force and yawing moment due to rolling arise, for attached flow, from two different sources, the first being due to the leading-edge suction forces, and the second from the components of the forces acting on wings with dihedral. When the flow separates from the leading edge, the suction forces are assumed to vanish, and so only the dihedral contribution remains. Thus, for body axes, we have

$$\left.\begin{aligned} y_{p0} &= -\frac{A\Gamma}{6} \\ n_{p0} &= -\frac{\Gamma}{2}\left(1 - \frac{4}{3}\frac{x_0}{c_0}\right) \end{aligned}\right\} \text{for a delta wing} \tag{19a}$$

and

$$\left.\begin{aligned} y_{p0} &= -\frac{A\Gamma}{6} \\ n_{p0} &= -\frac{19\Gamma}{70}\left(1 - \frac{35}{19}\frac{x_0}{c_0}\right) \end{aligned}\right\} \text{for a gothic wing} \tag{19b}$$

where y_{p0} differs from the American C_{Yp} used in Ref. 1 by a factor $\frac{1}{2}$, and x_0 is the distance of the centre of moments behind the wing apex.

In order to transform the derivatives to wind axes, the values of y_{r0}, l_{r0} and n_{r0} are needed (*see* Appendix I). These are derived in Section 4, and so for rolling about wind axes, we write

$$\left.\begin{aligned} y_p &= -\frac{A\Gamma}{6} \\ l_p &= -\frac{\pi A}{32} + (l_{r0} + n_{p0})\alpha \\ n_p &= n_{p0} + \left(\frac{\pi A}{32} - l_{r0}\alpha\right)\alpha \end{aligned}\right\} \tag{20}$$

where l_{r0} and n_{p0} depend upon planform, dihedral and centre-of-gravity position.

The experimental results available are for flat wings ($\Gamma = 0$), so that $n_{p0} = 0$. The comparison in Fig. 10 indicates that the value of l_{r0} is probably too large, and that the vortices must cause an increase in the magnitude of l_p at moderate incidences. The chain-dotted curves for n_p have been obtained from the relation $n_p = -l_{p\,\exp}\alpha$, (which holds for flat wings), and are seen to give satisfactory agreement for α up to 15°. Since experimental results for l_p are more readily available than for n_p, this relation gives a useful guide to values of n_p.

The effect of the leading-edge vortices does seem to be appreciable in the rolling motion, and is probably due to two changes from the attached flow, namely, the different basic pressure distribution on the wing at incidence, and the asymmetric strength and position of the two vortices on

the rolling wing. The latter problem has not been solved, even for the comparatively simple vortex system used by Brown and Michael[9], but the former may be approached in a similar way to that suggested by Gdaliahu[10] for wings of large aspect ratio.

Consider the slender wing at any spanwise station, distance x from the apex of the wing. The boundary condition on the wing is

$$0 = \alpha + \epsilon - \frac{w}{V} \tag{21}$$

where α is the incidence of the wing, ϵ is the additional incidence due to rolling, and w is the downwash due to the vortex system.

For attached flow,

$$w = \frac{1}{2\pi} \int_{-s}^{+s} \frac{d\Gamma}{dy'} \frac{dy'}{y - y'}$$

where s is the local semispan, and $\Gamma(y)$ is the vorticity distribution on the wing (*see* Ref. 11). However, this value of the downwash will be modified by the presence of the leading-edge vortices, and so we assume that

$$w = \frac{\lambda(y)}{2\pi} \int_{-s}^{+s} \frac{d\Gamma}{dy'} \frac{dy'}{y - y'} \tag{22}$$

where $\lambda(y)$ is an unknown function. This downwash is similar to that for the lifting-line theory, and so we may follow the analysis of Ref. 10.

We write

$$\left.\begin{aligned} \Gamma(y) &= 4sV \sum_{1}^{\infty} A_m \sin m\theta \\ y &= s \cos \theta \end{aligned}\right\} \tag{23}$$

so that

$$\frac{w}{V} = 2\lambda(\theta) \sum_{1}^{\infty} \frac{mA_m \sin m\theta}{\sin \theta}$$

and equation (21) gives that

$$0 = \alpha + \epsilon - 2\lambda(\theta) \sum_{1}^{\infty} \frac{mA_m \sin m\theta}{\sin \theta}. \tag{24}$$

Let $A_m = a_m\alpha + b_m$, and further assume that $\lambda(\theta)$ is independent of ϵ, so that we may separate equation (24) into two parts,

$$0 = 1 - 2\lambda(\theta) \sum_{1}^{\infty} \frac{ma_m \sin m\theta}{\sin \theta} \tag{25a}$$

and

$$0 = \epsilon - 2\lambda(\theta) \sum_{1}^{\infty} \frac{mb_m \sin m\theta}{\sin \theta}. \tag{25b}$$

If $\lambda(\theta) = 1$ for all θ, then we have the solution $a_1 = \frac{1}{2}$, $a_n = 0$ for $n \neq 1$, that is, the elliptic loading given by De Young[11]. If we have a more exact solution for the lift distribution due to uniform incidence α, then equation (25a) will give $\lambda(\theta)$, and equation (25b) may then be used to give the b_n's, the Fourier coefficients of the antisymmetric loading, i.e.

$$\frac{1}{\lambda(\theta)} = \frac{2 \sum_{1}^{\infty} ma_m \sin m\theta}{\sin \theta} = \frac{2 \sum_{1}^{\infty} mb_m \sin m\theta}{\epsilon \sin \theta}. \tag{26}$$

For rolling motion, the antisymmetric incidence is given by

$$\epsilon = \frac{py}{V} = \frac{ps\cos\theta}{V},$$

and so, on equating coefficients of $\sin n\theta$ in equation (26), we have

$$nb_n = \frac{ps}{2V}[(n-1)a_{n-1} + (n+1)a_{n+1}]. \tag{27}$$

To the first order in perturbation velocity, the pressure difference across the wing is given by

$$\Delta p = 2\rho V \frac{\partial \phi}{\partial x},$$

and the rolling moment due to this pressure difference is then

$$\begin{aligned} L &= -\int\int 2\rho V \frac{\partial \phi}{\partial x} y\, dy\, dx = -\int_{-b/2}^{+b/2} 2\rho V[\phi]_{\mathrm{TE}}\, y\, dy \\ &= -\rho V \int_{-b/2}^{+b/2} \Gamma(y) y\, dy = -\rho V^2 \left(\frac{b}{2}\right)^3 \pi A_2 \text{ on using equation (23)} \\ &= -\rho V^2 \left(\frac{b}{2}\right)^4 \frac{\pi}{4}(a_1 + 3a_3)\frac{pb}{2V}, \text{ from equation (27)}. \end{aligned} \tag{28}$$

Thus the damping-in-roll coefficient, referred to body axes, is

$$l_{p0} = \frac{1}{\frac{1}{2}\rho V^2 Sb}\frac{dL}{d\left(\frac{pb}{2V}\right)} = -\frac{\pi A}{16}(a_1 + 3a_3). \tag{29}$$

There are various sources available for evaluating the coefficients a_1 and a_3; as a check, it is seen that De Young's theory[11] gives $a_1 = \frac{1}{2}$, $a_3 = 0$, which leads to Ribner's[1] result, $l_{p0} = -\pi A/32$. There are at present three theories for slender delta wings with leading-edge separation, and some experimental load distributions have also been reported, so these have been used in the calculations.

(i) Küchemann[12] considers part-span vorticity on the wing surface in order to account for the breakaway at the leading edges. The theory gives an analytic solution for the a_n's,

$$\left.\begin{aligned} a_1 &= \frac{C_L}{\pi A \alpha} \\ \text{and} \qquad a_n &= \frac{C_L}{\pi A \alpha}\frac{2}{n(n^2-1)}\left\{\frac{n\cos n\theta_0}{\cos\theta_0} - \frac{\sin n\theta_0}{\sin\theta_0}\right\} \text{ for } n \text{ odd}, n \neq 1 \end{aligned}\right\} \tag{30}$$

where the suggested value for the parameter θ_0 is

$$\cos\theta_0 = 1 - \frac{2\alpha}{\pi}. \tag{31}$$

The value of l_{p0} is then given by

$$l_{p0} = -\frac{\pi A}{16}\frac{C_L}{\pi A\alpha}\cos 2\theta_0 = -\frac{C_L}{16\alpha}\left(1-\frac{8\alpha}{\pi}+\frac{8\alpha^2}{\pi^2}\right). \tag{32}$$

(ii) There are two theories which represent the leading-edge separation by vorticity distributions above the wing[9,13], but as the latter approach, due to Mangler and Smith, is the more accurate of the two, the a_n's were evaluated from the load distributions shown in Fig. 8 of Ref. 13. Here the load, $L(y) = 2\Gamma(y)/V$, is given in the form $KL(y)/sC_N$ as a function of α/K, where $K = A/4$ and C_N = normal-force coefficient. C_N/K^2 is also a function of α/K, and so finally we find that

$$a_n = \frac{C_N}{K^2}\frac{K}{\alpha}\frac{1}{\pi}\int_0^\pi \frac{KL(y)}{sC_N}\sin n\theta\, d\theta. \tag{33}$$

The final result for l_{p0}/A is given in the accompanying table.

α/K	0	0·25	0·5	1·0	2·5
l_{p0}/A	−0·098	−0·165	−0·163	−0·132	−0·019

(iii) Experimental values of $L(y)$ are given in Ref. 14 for a delta wing of aspect ratio 0·705. The a_1 and a_3 have been evaluated, using equation (30), and the results for l_{p0} are given below.

α/K	0	0·25	0·5	1·0	2·5
l_{p0}/A			−0·099	−0·047	−0·028

The results from the three loadings are shown in Fig. 11a, together with Ribner's attached-flow result, for a delta wing of aspect ratio 1·0, with l_p referred to body axes. The loadings from experiment, and from Mangler and Smith's theory, do indicate an initial increase in the magnitude of l_{p0}, followed by a decrease as α increases further. The transformation to wind axes, using the l_{r0} derived in the following section, leads to the results shown in Fig. 11b. Again it appears that l_{r0} is too large for all the loadings. The effect of the vortices at moderate incidences ($< 10°$) is overestimated by the Mangler and Smith loading, and further attempts at estimating l_p will have to consider the effect of the asymmetric values of the strength and position of the vortices caused by the rolling of the wing.

4. *The Derivatives Due to Yawing.*

The value of l_r given in Ref. 1 is applicable to wings of very small aspect ratio, for which A may be neglected in comparison with $1/A$. This approximation is not valid for the wings under current consideration, and so the complete expression for the rolling moment due to yawing must be used (as in Ref. 15),

$$L = -\iint 2\rho\left[(V-ry)\frac{\partial\phi}{\partial x}+r(x-x_0)\frac{\partial\phi}{\partial y}\right] y\, dy\, dx \tag{34}$$

where x_0 is the distance of the centre of moments behind the wing apex, and ϕ is the velocity potential due to a wing at incidence α.

For attached flow, equation (34) gives

$$\left.\begin{aligned} l_{r0} &= \frac{\pi A\alpha}{16} + \left(1 - \frac{4}{3}\frac{x_0}{c_0}\right)\frac{\pi\alpha}{A} + \frac{2\Gamma}{3}\left(1 - \frac{x_0}{c_0}\right) \quad \text{for a delta wing} \\ l_{r0} &= \frac{\pi A\alpha}{16} + \left(\frac{33}{40} - \frac{6}{5}\frac{x_0}{c_0}\right)\frac{\pi\alpha}{A} + \frac{2\Gamma}{3}\left(1 - \frac{x_0}{c_0}\right) \quad \text{for a gothic wing} \end{aligned}\right\} \tag{35}$$

If the wings are thin, we may assume that the profile drag is small, so that, in body axes, $n_{r0} \approx 0$. In wind axes, we then have that

$$\left.\begin{aligned} l_r &= l_{r0} - l_{p0}\alpha \\ &= \frac{3\pi A\alpha}{32} + \left(1 - \frac{4}{3}\frac{x_0}{c_0}\right)\frac{\pi\alpha}{A} + \frac{2\Gamma}{3}\left(1 - \frac{x_0}{c_0}\right) \quad \text{for a delta wing} \\ &= \frac{3\pi A\alpha}{32} + \left(\frac{33}{40} - \frac{6}{5}\frac{x_0}{c_0}\right)\frac{\pi\alpha}{A} + \frac{2\Gamma}{3}\left(1 - \frac{x_0}{c_0}\right) \quad \text{for a gothic wing} \end{aligned}\right\} \tag{36}$$

and

$$\begin{aligned} n_r &= -\left[\frac{3\pi A\alpha}{32} + \left(1 - \frac{4}{3}\frac{x_0}{c_0}\right)\frac{\pi\alpha}{A} + \frac{\Gamma}{6}\right]\alpha \quad \text{for a delta wing} \\ &= -\left[\frac{3\pi A\alpha}{32} + \left(\frac{33}{40} - \frac{6}{5}\frac{x_0}{c_0}\right)\frac{\pi\alpha}{A} + \Gamma\left(\frac{83}{210} - \frac{x_0}{6c_0}\right)\right]\alpha \quad \text{for a gothic wing} \\ &= -l_r\alpha \text{ for all planforms when } \Gamma = 0. \end{aligned} \tag{37}$$

The experimental results available (Ref. 3 for the oscillatory l_r and n_r of a series of delta wings, and Ref. 16 for the oscillatory n_r of a delta and two gothic wings) are very erratic, showing large variations with frequency. Fig. 12 shows some of the American results, together with the theoretical values given by equations (36) and (37), but it is impossible to draw any conclusions as to the degree of accuracy of the theory.

From equation (34), it may be seen that the rolling moment arises from two different effects of yawing, the first term being due to an effective forward velocity, $V - ry$, and the second term to an effective sideslip velocity $r(x - x_0)$. We have seen that the leading-edge vortices have little effect on the sideslip derivatives, and so we assume that the second term is unchanged in separated flow. The contribution of the first term to the rolling moment, L_1 say, is given by

$$\begin{aligned} L_1 &= -\int\int 2\rho(V - ry)\frac{\partial\phi}{\partial x} y\, dy\, dx = -\int_{-b/2}^{+b/2} \rho(V - ry)\Gamma(y) y\, dy \\ &= \rho V\left(\frac{b}{2}\right)^4 \frac{\pi}{2}(a_1 + a_3)\alpha r \end{aligned} \tag{38}$$

in the notation of Section 3. The corresponding contribution to the derivative, l_{1r} say, is thus

$$l_{1r} = \frac{\pi A}{8}(a_1 + a_3)\alpha \tag{39}$$

which now replaces the term $\pi A\alpha/16$ in equations (35). The a_1 and a_3 calculated from the various loadings discussed in Section 3 were used to give values for l_{1r}. The results are:

(i) Küchemann's loading[12]

$$l_{1r} = \frac{C_L}{8}\left\{1 - \frac{8\alpha}{3\pi} + \frac{8\alpha^2}{3\pi^2}\right\}. \tag{40}$$

(ii) Mangler and Smith's loading[13]

α/K	0	0·25	0·5	1·0	2·5
$l_{1r}/A\alpha$	0·196	0·263	0·284	0·303	0·276

(iii) Experimental loading[14]

α/K	0	0·25	0·5	1·0	2·5
$l_{1r}/A\alpha$			0·245	0·233	0·286

These values were used to give l_{r0}, required for the transformation of l_{p0} to wind axes {equation (20)} for the comparison in Fig. 11b, and the results for l_r obtained using the Mangler-and-Smith loading are shown in Fig. 12, in comparison with results from experiment and attached-flow theory.

5. *Fin Contributions to the Derivatives.*

5.1. *The Derivatives Due to Sideslip.*

As stated in the Introduction, the fins envisaged at the moment for aircraft with slender wings are of comparatively simple shape, and their effectiveness may be estimated by considering the wing to be a total reflection plate. For the sideslip derivatives, the lift-curve slope and chordwise position of the aerodynamic centre of the planform derived by reflecting the exposed fin area in the wing surface may be obtained from the Data Sheets of the Royal Aeronautical Society[27].
Then

$$y_{v\,\mathrm{Fin}} = -\frac{1}{2}\left(\frac{dC_L}{d\alpha}\right)_{\mathrm{Fin}}\frac{S_F}{S} \tag{41}$$

where S_F is the net area of the fin, and S is the area of the wing,
and

$$n_{v\,\mathrm{Fin}} = -\frac{x_F}{s_w}\,y_{v\,\mathrm{Fin}} \tag{42}$$

where x_F is the distance of the aerodynamic centre of the fin behind the centre of moments, and s_w is the semispan of the wing. When the wing is at incidence, we have that

$$x_F = x_{F0} + z_{F0}\alpha \tag{43}$$

where x_{F0} is the distance of the aerodynamic centre of the fin behind the centre of moments, measured along the centre line of the wing, and z_{F0} is the height of the centre of pressure of the fin above the root chord of the fin. For triangular fins, we assume that

$$z_{F0} = \tfrac{1}{3}s_F, \tag{44}$$

where s_F is the height of the fin.
Similarly,

$$\left.\begin{aligned} l_{v\,\mathrm{Fin}} &= \frac{z_F}{s_w}\,y_{v\,\mathrm{Fin}} \\ z_F &= z_{F0} - x_{F0}\alpha. \end{aligned}\right\} \tag{45}$$

where

A series of experiments by Kirby at the R.A.E. give a useful comparison with the theoretical results obtained from the above analysis, and from slender-body theory[2]. The wing tested was a flat-plate delta, with $A = 1{\cdot}0$, and with three different fins, as shown in Fig. 13a, which all had the same fin height, but different chords. For fins of practical size, i.e. $S_F/S \leqslant 0{\cdot}2$, the slender-body theory overestimates $y_{v\,\mathrm{Fin}}$ and $n_{v\,\mathrm{Fin}}$ as might be expected, but gives good agreement for the largest fin, which is the most slender of the three. The estimates based on equations (41) and (42) give good agreement up to incidences of 15°. The $l_{v\,\mathrm{Fin}}$, is not quite so good (Fig. 13d), but the error is negligible when compared to the contribution to l_v from the wing at incidence. The configuration was also tested with the wing at 20° anhedral, and for these the estimate based on the reflected fin is not so satisfactory. The experiment shows that the fin becomes more effective on the wing with anhedral, and that its effectiveness increases as the incidence of the wing increases, suggesting the existence of sidewash effects which have not been accounted for in the theory.

The results for 60° delta fins tested by Avro[18], on a gothic wing of aspect ratio $0{\cdot}75$, are also compared with the theoretical estimates in Fig. 14, and show remarkable agreement up to angles of incidence of 15°, both for single fins, and for twin fins of various sizes.

5.2. *The Derivatives Due to Rolling.*

The incidence distribution on the reflected fin, taken as a wing rolling about its centreline chord, is $w = p|y|$, where y is the ordinate along the span, and so the lift and moments have to be evaluated by a lifting-surface method. Miss Klanfer at the R.A.E. used the Bristol programme on DEUCE for Multhopp's theory[17] on a 60° delta wing, and these results have been used to calculate the contribution to the derivatives from the fin.

If $dC_L/d(ps_F/V)$ is the lift-curve slope due to the rate of roll, then the derivatives are

$$\left.\begin{aligned} y_{p\,\mathrm{Fin}} &= -\left[\frac{1}{2}\right]\frac{dC_L}{d(ps_F/V)}\frac{s_F}{s_w}\frac{S_F}{S} \\ l_{p\,\mathrm{Fin}} &= \frac{z_{pF}}{s_w}\,y_{p\,\mathrm{Fin}} \\ n_{p\,\mathrm{Fin}} &= -\frac{x_{pF}}{s_w}\,y_{p\,\mathrm{Fin}} \end{aligned}\right\} \text{ referred to body axes} \qquad (46)$$

where z_{pF} and x_{pF} for the rolling fin correspond to the z_{p0} and x_{p0} for the sideslipping fin, and are evaluated from the lift distribution and pitching moment respectively. The transformation to wind axes involves more than measuring the z_{pF} and x_{pF} relative to the wind direction, as was possible for the sideslip moment arms, {equations (43) and (45)} since the rolling axis has also to be transformed. The formulae for the transformations are

$$\left.\begin{aligned} l_p &= l_{p0}(1-\alpha^2) + (l_{r0}+n_{p0})\alpha + n_{r0}\alpha^2 \\ n_p &= n_{p0}(1-\alpha^2) + (n_{r0}-l_{p0})\alpha - l_{r0}\alpha^2 \end{aligned}\right\} \qquad (47)$$

and so we require the derivatives due to yawing, as given in the following section, equations (52).

As may be seen from Fig. 15, where the Avro experimental results for the same fins as shown in Fig. 14 are compared with equation (47), the theory underestimates the fin contributions. This is probably due to the effect of the sidewash on the fin arising from the vorticity distribution on the wing, and the leading-edge vortices. The sidewash due to the antisymmetric vorticity distribution

on the rolling wing may be evaluated, using attached-flow theory, in a similar manner to that suggested by Michael[20] for wing and tailplane configurations. The sidewash velocity on a centrally placed fin is given by

$$v = \left(\frac{\partial \phi}{\partial y}\right)_{y=0} \tag{48}$$

where, from Ref. 26

$$\left.\begin{aligned} \phi &= \tfrac{1}{4} p s^2 e^{-2\xi} \sin 2\eta \\ y &= s \cosh \xi \cos \eta \\ z &= s \sinh \xi \sin \eta \end{aligned}\right\}, \tag{49}$$

i.e.

$$v = \frac{ps}{2}\left[\frac{1 + 2z^2/s^2}{(1+z^2/s^2)^{1/2}} - \frac{2z}{s}\right].$$

The contribution of the sidewash to the derivatives is most easily estimated by considering the average value of the sidewash angle $\sigma = v/V$ over the height of the fin, which leads to

$$\left(\frac{\partial \sigma}{\partial \dfrac{pb}{2V}}\right)_{\text{av}} = \frac{s}{b}\left[\left(1 + \frac{h^2}{s^2}\right)^{1/2} - \frac{h}{s}\right] \tag{50}$$

where h is the local height of the fin, and s is the local semispan of the wing, measured at the chordwise position of the centre of pressure of the fin.

Then, in wind axes, the increments in the rolling derivatives due to the sidewash from the wing are given by

$$\left.\begin{aligned} \Delta l_{p\,\text{Fin}} &= -y_{p\,\text{Fin}}\left(\frac{z_{pF}}{s_w} - \frac{x_{pF}}{s_w}\alpha\right)\left(\frac{\partial \sigma}{\partial \dfrac{pb}{2V}}\right)_{\text{av}} \\ \Delta n_{p\,\text{Fin}} &= y_{p\,\text{Fin}}\left(\frac{x_{pF}}{s_w} + \frac{z_{pF}}{s_w}\alpha\right)\left(\frac{\partial \sigma}{\partial \dfrac{pb}{2V}}\right)_{\text{av}} . \end{aligned}\right\} \tag{51}$$

Including these sidewash terms does improve the estimate for $n_{p\,\text{Fin}}$, *see* Fig. 15, but when the wing is at incidence, it is obvious that the sidewash due to the leading-edge vortices must also be taken into account. Since this sidewash depends on the asymmetric strength and position of these vortices, the basic problem of a slender wing in an antisymmetric flow must be solved before a satisfactory estimate of fin effectiveness in roll can be obtained.

5.3. *The Derivatives Due to Yawing.*

The yawing motion of the fin may be considered to be equivalent to a pitching motion of the planform derived by reflecting the fin in the wing surface, if sidewash effects are neglected. For triangular planforms, the charts of Ref. 21 may be used, and estimates for sweptback untapered wings are given in Ref. 22, so that interpolation is necessary for intermediate taper ratios. For the rolling moment, the lift distribution due to steady pitch of a 60° delta wing, obtained using Multhopp's lifting-surface theory[17], gives a moment arm of $0{\cdot}36 s_F$, and so a good approximation for most fins would be $\frac{1}{3} s_F$. It is probably most convenient to evaluate the force and moment derivatives for an axis through the fin apex, changing the reference area and length from fin area

and fin mean chord to wing area and wing semispan before transforming the axis of rotation to the centre of moments of the aircraft. If the suffix 'a' refers to the derivative of the fin, due to rotation about an axis through the fin apex, which is a distance x_a behind the centre of moments, then, about body axes,

$$\left.\begin{aligned} y_{r\,\mathrm{Fin}} &= y_{ra} - \frac{x_a}{s} y_{v\,\mathrm{Fin}} \\ l_{r\,\mathrm{Fin}} &= l_{ra} - \frac{x_a}{s} l_{v\,\mathrm{Fin}} \approx \tfrac{1}{3} \frac{s_F}{s} y_{r\,\mathrm{Fin}} \\ n_{r\,\mathrm{Fin}} &= n_{ra} - \frac{x_a}{s}(y_{ra} + n_{va}) + \left(\frac{x_a}{s}\right)^2 y_{v\,\mathrm{Fin}}. \end{aligned}\right\} \tag{52}$$

The transformation to wind axes is obtained using the equations in Appendix I, together with the rolling derivatives derived in Section 5.2. The available experimental results are all for oscillatory damping-in-yaw, $n_r - n_{\dot{v}}$, and this derivative may be estimated from the equivalent oscillatory pitching motion, in a similar way to that described above for the steady motion. The charts of Ref. 21 give the equivalent damping-in-pitch, $m_{\dot{\vartheta}}$, for delta wings but for other planforms the Multhopp calculation for oscillating wings would have to be used[23], from which may be derived the value of $m_{\dot{\vartheta}}$ about the axis through the centre of moments of the aircraft. Then, converting the reference areas and lengths, the damping-in-yaw, referred to body axes, is

$$(n_r - n_{\dot{v}})_{0\,\mathrm{Fin}} = m_{\dot{\vartheta}} \frac{S_F}{S} \frac{\bar{c}_F{}^2}{s^2}. \tag{53}$$

For the transformation to wind axes, the oscillatory rolling derivatives should be used, but Gray has shown experimentally, in some unpublished work at the R.A.E., that there is no significant difference between the steady and oscillatory values of l_p, and so the estimated steady values were used. It has also to be assumed that $l_{\dot{v}} \approx 0$, so that

$$(n_r - n_{\dot{v}}) = (n_r - n_{\dot{v}})_0 (1 - \alpha^2) - (l_{r0} + n_{p0})\alpha + l_{p0}\alpha^2 \tag{54}$$

from Appendix I.

The comparison with experimental results, from Ref. 16, is shown in Fig. 16; the Bristol results are for the fins shown in Fig. 14. The theoretical estimate is seen to be quite good for incidences up to 15°, but the loss in damping at higher incidences is not predicted. Similar agreement is obtained with Gray's unpublished results for 60° delta fins on a delta wing with rounded tips (Fig. 16b).

6. *Conclusions.*

The theoretical estimates for the sideslip derivatives for slender wings with fins are shown to be in good agreement with experimental results, and a second-order semi-empirical formula is derived for the anhedral effect on l_v due to drooping the tips of delta wings. However, it should be noted that this formula does not extend to the ogee wing which has been tested, where l_v becomes markedly non-linear with α. For the derivatives due to rolling, estimates cannot be given so confidently, and further work needs to be done on the effect of the leading-edge vortices on the wing and on the fin when the rolling of the wing causes an asymmetry in the strength and position of the vortices. The assessment is also complicated by the fact that the wind-tunnel measurements have been made for wings rolling about the wind axes, so that the theoretical estimation involves the value of l_{r0}, for

which no reliable experimental check is available. The damping-in-yaw of the wing and fin is satisfactorily given by theory for incidences up to about 15°, but the loss in damping at higher incidences is not predicted.

7. *Future Work.*

Although it has been shown that reasonable estimates for the sideslip derivatives may be obtained by neglecting the effects of leading-edge separations, it is obviously necessary to seek to understand why this is so. For the rotary derivatives, the influence of the vortices is not adequately estimated by the present theory at large incidences, and, as stated in the text, more exact methods of calculating the flow field are needed. The main problem is the calculation of the strength and position of the leading-edge vortices when the wing is moving laterally, and as a first step to the solution, an attempt is being made to extend the lifting-surface theory of Ref. 12. Other factors which must be considered are the effects of change of planform (e.g. to ogee wings) and the effects, both direct and from interference, due to mounting the wing on a body.

Some experimental results at supersonic speeds for the sideslip derivatives are now available, and estimates are being made for comparison. Since flight at high speeds will necessarily be at small incidences, the effect of the leading-edge separation will not be so important as in the low-speed, high incidence case which is the main interest of this present report.

Acknowledgement.

The author wishes to acknowledge the help and guidance given by Mr. H. H. B. M. Thomas during the course of this investigation, and the assistance given by Miss F. M. Ward, Mrs. G. Helyer and Mr. J. T. Webb in the computational work.

LIST OF SYMBOLS

A		Aspect ratio
A_n, B_n a_n, b_n		Fourier coefficients
b		Span
C_N		Normal-force coefficient
$\left(\frac{dC_L}{d\alpha}\right)_{\text{Fin}}$		Lift-curve slope of fin due to incidence
$\frac{dC_L}{d(ps_F/V)}$		Lift-curve slope of fin due to rolling
c_0		Root chord of wing
$\bar{c}_F$		Mean chord of fin
h		Local semi-thickness of diamond cross-section (Section 2.2) Height of fin at centre of pressure (Section 5.2)
K	=	$A/4$ for delta wings
L		Rolling moment
$L(y)$		Load distribution
$n_r - n_{\dot{v}}$		Oscillatory damping-in-yaw coefficient
Δp		Pressure difference
p		Angular velocity in roll, radians per second
q		Angular velocity in pitch, radians per second
r		Angular velocity in yaw, radians per second
r_0		Parameter used in Section 2.2
S		Area of wing
S_F		Net area of fin
s		Local semispan of wing
s_w		Semispan of wing at trailing edge
s_F		Height of fin
t		Thickness of wing
V		Forward velocity
v		Velocity in y-axis direction
w		Downwash velocity
x		Chordwise co-ordinate, along wind or body axes

x_a		Distance of apex of fin from centre of moments, measured along the chord of the wing
x_0		Distance of centre of moments behind wing apex
y		Spanwise co-ordinate
z		Co-ordinate normal to $x - y$ plane
x_{F0}, z_{F0}		Co-ordinates of centre of pressure due to incidence on fin, in body axes
x_{pF}, z_{pF}		Co-ordinates of centre of pressure due to rolling on fin, in body axes
α		Angle of incidence, radians
β		Angle of sideslip, radians
γ, Γ		Angles of anhedral and dihedral, radians
$\gamma_1, \gamma_2, \Gamma_1, \Gamma_2$		Anhedral-dihedral distribution across the span (*see* Fig. 3)
$\Gamma(y)$		Spanwise distribution of vorticity
Γ		Gamma-function (Section 2.2)
ϵ		Effective incidence due to rolling
ζ	$=$	$y + iz$, physical plane
θ	$=$	$\cos^{-1}(y/s)$
θ_0		Parameter used in Section 3
λ		Inboard fraction of semispan for a wing with part-span dihedral
$\lambda(y)$		Function introduced in equation (22)
ρ		Density
σ		Transformation plane (Section 2.2) Sidewash velocity (Section 5.2)
τ	$=$	$\tan^{-1}(h/s)$ for wing with diamond cross-section
ϕ		Velocity potential
ξ, η		Co-ordinates in transformation plane

The derivatives are as defined in R. & M. 1801

Suffixes

0	Derivative referred to body axes
1	Part of l_r due to effective incidence
TE	Trailing edge
Fin	Contribution of fin to derivative

REFERENCES

No.	*Author(s)*	*Title, etc.*
1	H. S. Ribner	The stability derivatives of low-aspect-ratio triangular wings at subsonic and supersonic speeds. N.A.C.A. Tech. Note 1423. September, 1947.
2	A. H. Sacks	Aerodynamic forces, moments and stability derivatives for slender bodies of general cross section. N.A.C.A. Tech. Note 3283. November, 1954.
3	W. Letko	Experimental determination at subsonic speeds of the oscillatory and static lateral stability derivatives of a series of delta wings with leading-edge sweep from 30° to 86·5°. N.A.C.A. Research Memo. L57A30. TIL/5487. April, 1957.
4	D. H. Peckham	Low-speed wind-tunnel tests on a series of uncambered slender pointed wings with sharp edges. A.R.C. R. & M. 3186. December, 1958.
5	M. B. Howard	An investigation into the low-speed aerodynamic characteristics of a family of slender wings. Part II—A comparison of the static stability of three gothic wings and a delta wing. Avro Report ARD/WT/735/3. 1958.
6	W. J. G. Trebble	Experimental reduction of the rolling moments on a delta wing of aspect ratio 1·0 at low speeds by applying either full span anhedral or deflecting the wing tips. Unpublished M.o.A. Report.
7	J. B. Scott-Wilson	An investigation into the low-speed aerodynamic characteristics of a family of slender wings. Part I—The measurement of the rolling derivatives of three gothic wings and a delta wing. Avro Report ARD/WT/735/2. 1958.
8	R. L. Maltby and A. M. Hay ..	Tests on a thin ogee wing with drooped tips. Unpublished M.o.A. Report.
9	C. E. Brown and W. H. Michael..	On slender delta wings with leading edge separation. *J. Ae. Sci.*, Vol. 21. 1954.
10	M. Gdaliahu	The lift increment of an aerofoil due to variation of incidence along the span and a simple method of estimating the lift distribution. A.R.C. R. & M. 2261. December, 1945.
11	J. De Young	Spanwise loading for wings and control surfaces of low aspect ratio. N.A.C.A. Tech. Note 2011. January, 1950.
12	D. Küchemann	A non-linear lifting-surface theory for wings of small aspect ratio with edge separations. R.A.E. Report Aero. 2540. A.R.C. 17 769. April, 1955.
13	K. W. Mangler and J. H. B. Smith	Calculation of flow past slender delta wings with leading edge separation. *Proc. Roy. Soc.* A, Vol. 251, p. 200. May, 1959.
14	P. T. Fink	Further experiments with 20 degree delta wings. A.R.C. 19 526. September, 1957.

REFERENCES—*continued*

No.	*Author(s)*	*Title, etc.*
15	H. S. Ribner and F. S. Malvestuto	Stability derivatives of triangular wings at supersonic speeds. N.A.C.A. Tech. Note 1572. May, 1948.
16	J. C. Wright and T. W. Nicholls..	Low speed wind tunnel measurement of oscillatory derivatives for a family of slender wings. Part I—Damping in yaw. Bristol Report W.T.337. 1959.
17	H. Multhopp	Methods for calculating the lift distribution of wings (subsonic lifting-surface theory). A.R.C. R. & M. 2884. January, 1950.
18	M. B. Howard	An investigation into the low-speed aerodynamic characteristics of a family of slender wings. Part V—A comparison of the lateral stability derivatives of a gothic wing with various fin configurations. Avro Report ARD/WT/735/8. 1959.
19	M. A. Hundleby	An investigation into the low-speed aerodynamic characteristics of a family of slender wings. Part III—The measurement of rolling derivatives on a gothic wing fitted with various fins, on a gothic and a delta wing fitted with leading edge extensions, and on a gothic wing fitted with conical camber. Avro Report ARD/WT/735/5. 1959.
20	W. H. Michael	Analysis of the effects of wing interference on the tail contributions to the rolling derivatives. N.A.C.A. Report 1086. 1952.
21	H. H. B. M. Thomas and B. F. R. Spencer.	The calculations of the derivatives involved in the damping of the longitudinal short period oscillations of an aircraft and correlation with experiment. R.A.E. Report Aero. 2561. A.R.C. 18 498. November, 1955.
22	T. A. Toll and M. J. Queijo ..	Approximate relations and charts for low-speed stability derivatives of swept wings. N.A.C.A. Tech. Note 1581. May, 1948.
23	H. C. Garner	Multhopp's subsonic lifting surface theory of wings in slow pitching oscillations. A.R.C. R. & M. 2885. July, 1952.
24	V. M. Falkner	The design of minimum drag tip fins. With an appendix: On the conformal transformation of a wing with a fin, by Sir Charles Darwin. A.R.C. R. & M. 2279. March, 1945.
25	J. W. Paulson	Comparison of the static stability of a 68·7° delta wing model with dihedral and a twisted and cambered wing model of the same planform. N.A.C.A. Research Memo. L55B11. TIB/4651. April, 1955.
26	H. Lamb	*Hydrodynamics.* Chapter IV. Cambridge University Press. 1924.
27	—	Data Sheets. Aerodynamics Vol. II. Wings 01.01.01 and S.01.03.03 to .06 and Wings 08.01.01 and S.08.01.02. Royal Aeronautical Society.

APPENDIX I

Formulae for the transformation of the lateral stability derivatives

(i) Formulae for the transformation of the lateral stability derivatives from body to wind-body axes.

$$y_v = y_{v0}$$

$$y_p = y_{p0}\cos\alpha + y_{r0}\sin\alpha$$

$$y_r = y_{r0}\cos\alpha - y_{p0}\sin\alpha$$

$$l_v = l_{v0}\cos\alpha + n_{v0}\sin\alpha$$

$$l_p = l_{p0}\cos^2\alpha + (l_{r0}+n_{p0})\sin\alpha\cos\alpha + n_{r0}\sin^2\alpha$$

$$l_r = l_{r0}\cos^2\alpha + (n_{r0}-l_{p0})\sin\alpha\cos\alpha - n_{p0}\sin^2\alpha$$

$$n_v = n_{v0}\cos\alpha - l_{v0}\sin\alpha$$

$$n_p = n_{p0}\cos^2\alpha + (n_{r0}-l_{p0})\sin\alpha\cos\alpha - l_{r0}\sin^2\alpha$$

$$n_r = n_{r0}\cos^2\alpha - (l_{r0}+n_{p0})\sin\alpha\cos\alpha + l_{p0}\sin^2\alpha.$$

(ii) Formulae for the transformation of the lateral stability derivatives to a new origin of axes, displaced by distances Δx and Δz (positive forward and down respectively).

$$y'_{v'} = y_v$$

$$y'_{p'} = y_p + \frac{\Delta z}{s}y_v$$

$$y'_{r'} = y_r - \frac{\Delta x}{s}y_v$$

$$l'_{v'} = l_v + \frac{\Delta z}{s}y_v$$

$$l'_{p'} = l_p + \frac{\Delta z}{s}(l_v+y_p) + \left(\frac{\Delta z}{s}\right)^2 y_v$$

$$l'_{r'} = l_r + \frac{\Delta z}{s}y_r - \frac{\Delta x}{s}l_v - \frac{\Delta x}{s}\frac{\Delta z}{s}y_v$$

$$n'_{v'} = n_v - \frac{\Delta x}{s}y_v$$

$$n'_{p'} = n_p - \frac{\Delta x}{s}y_p + \frac{\Delta z}{s}n_v - \frac{\Delta x}{s}\frac{\Delta z}{s}y_v$$

$$n'_{r'} = n_r - \frac{\Delta x}{s}(y_r+n_v) + \left(\frac{\Delta x}{s}\right)^2 y_v$$

where s = semispan of wing.

APPENDIX II

Evaluation of l_v for Wings with Tips Drooped through 90°

The transformation planes are shown in Fig. 17. The ζ-plane is a section across the span, and this is rotated through 90°, so that the z-plane is symmetrical about its real axis

$$z = i\zeta. \tag{55}$$

The Schwarz-Christoffel transformation to the upper half of the t-plane is

$$\frac{dz}{dt} = \frac{M(t-b_2)\,(t-a_2)^{1/2}}{[(t-a_1)\,(t-a_3)\,(t-a_4)]^{1/2}} \tag{56}$$

but it is easier to consider the more general transformation

$$\frac{dz}{dt} = \frac{M(t-b_1)\,(t-b_2)}{[(t-a_1)\,(t-a_2)\,(t-a_3)\,(t-a_4)]^{1/2}} \tag{57}$$

and then use the Appendix of Ref. 24 for the integration. The substitution used there is

$$t = \frac{a\,\mathrm{sn}\,u + b}{c\,\mathrm{sn}\,u + d} \tag{58}$$

and then equation (57) becomes

$$\frac{dz}{du} = \frac{N(\mathrm{sn}\,u-\mu_1)\,(\mathrm{sn}\,u-\mu_2)}{(\mathrm{sn}\,u-\nu)^2} \tag{59}$$

where

$$\left.\begin{aligned} &\mu_1 = \frac{-b+b_1d}{a-b_1c}, \qquad \mu_2 = \frac{-b+b_2d}{a-b_2c}, \qquad \nu = \frac{-d}{c} \\ &\text{and} \\ &N = M(ad-bc)\,(a-b_1c)\,(a-b_2c)/c^2. \end{aligned}\right\} \tag{60}$$

Integration of equation (59) gives

$$\frac{z}{s} = \frac{2\lambda K}{\pi}\left\{E(u) - \frac{E}{K}u + \frac{\mathrm{cn}\,u\,\mathrm{dn}\,u}{\mathrm{sn}\,u-\nu}\right\} \tag{61}$$

where the coefficient of the elliptic integral of the third kind has been made to vanish, and the relationship between the corresponding points in the z and u planes have been satisfied. These conditions are:

$$2\nu - \mu_1 - \mu_2 + \frac{\nu(\nu-\mu_1)\,(\nu-\mu_2)}{(1-\nu^2)\,(1-k^2\nu^2)}\,(1+k^2-2k^2\nu^2) = 0 \tag{62}$$

$$\left.\begin{aligned} a_4 &= \frac{a+b}{c+d}, \qquad a_1 = \frac{b-a}{c-d} \\ K\left[1 + \frac{(\nu-\mu_1)\,(\nu-\mu_2)}{(1-\nu^2)}\right] &= \frac{E(\nu-\mu_1)\,(\nu-\mu_2)}{(1-\nu^2)\,(1-k^2\nu^2)} \end{aligned}\right\} \tag{63}$$

$$\left.\begin{aligned} a_3 &= \frac{a+kb}{c+kd}, \qquad a_2 = \frac{a-kb}{c-kd} \\ \frac{N(\nu-\mu_1)\,(\nu-\mu_2)}{s(1-\nu^2)\,(1-k^2\nu^2)} &= -\frac{2\lambda K}{\pi} \end{aligned}\right\} \tag{64}$$

$$b_2 = \frac{a + bk\,\mathrm{sn}\,g}{c + dk\,\mathrm{sn}\,g}$$

and

$$(1-\lambda) = \frac{2\lambda K}{\pi}\left\{E(g) - \frac{\nu k\,\mathrm{cn}\,g\,\mathrm{dn}\,g}{1-\nu k\,\mathrm{sn}\,g} - \frac{Eg}{K}\right\}. \qquad (65)$$

We are free to choose two points in the t-plane, and so we put

$$a_1 = -2r_0 \qquad a_4 = +2r_0 \qquad (66)$$

which will be convenient for the transformation to a circle of radius r_0 in the σ-plane, required by Sacks[2].

Thus, from equations (62) to (66), we find that

$$a_3 = \frac{2r_0(k-\nu)}{1-\nu k} \qquad a_2 = b_1 = \frac{-2r_0(\nu+k)}{1+\nu k}$$

$$\mu_1 = \frac{-1}{k}, \qquad \mu_2 = (1+\nu k-\nu^2k^2-\nu^3k)/(k+\nu-\nu^2k-\nu^3k^2) \qquad (67)$$

$$\nu = \frac{1}{k}\left[\frac{K}{E}(1-k^2) - 1\right]$$

and also

$$\mu_2 = \frac{1}{k\,\mathrm{sn}\,g}.$$

For the numerical solution of these equations, it is better to work with the ϑ-functions, choosing the parameter q.

Then

$$\vartheta_2 = 2q^{1/4}(1+q^2+q^6+\ldots)$$

$$\vartheta_3 = 1 + 2q + 2q^4 + 2q^9 + \ldots \qquad (68)$$

$$k = \vartheta_2^2/\vartheta_3^2.$$

The values of ν and sn g are given by equation (67). The elliptic functions may also be expressed in terms of the ϑ-functions, and we have to use the relationships:

$$\mathrm{sn}\,g = \frac{\vartheta_3}{\vartheta_2}\frac{\vartheta_1(G)}{\vartheta_4(G)} \qquad \text{where} \qquad G = \frac{g\pi}{2K} = \frac{g}{\vartheta_3^2} \qquad (69)$$

and

$$\vartheta_1(G) = 2q^{1/4}(\sin G - q^2\sin 3G + q^6\sin 5G + \ldots)$$

$$\vartheta_4(G) = 1 - 2q\cos 2G + 2q^4\cos 4G - \ldots \qquad (70)$$

These equations have to be solved by an interation process, to give G.

Then

$$E(g) - g\frac{E}{K} = \frac{\pi}{2K}\frac{\vartheta_4'(G)}{\vartheta_4(G)} \qquad (71)$$

where

$$\vartheta_4'(G) = 4q\sin 2G - 8q^4\sin 4G + \ldots \qquad (72)$$

and so equation (65) gives that

$$\frac{1-\lambda}{\lambda} = \frac{\vartheta_4'(G)}{\vartheta_4(G)} - \frac{2K}{\pi}\nu k \frac{\operatorname{cn} g \operatorname{dn} g}{1-\nu k \operatorname{sn} g} \tag{73}$$

where

$$\operatorname{cn}^2 g = 1 - \operatorname{sn}^2 g \qquad \text{and} \qquad \operatorname{dn}^2 g = 1 - k^2 \operatorname{sn}^2 g . \tag{74}$$

Thus we find the ratio $(1-\lambda)/\lambda$ in terms of q, and so for a given λ we have to interpolate to find q, and then evaluate the constants in the transformations.

The t-plane must now be transformed to the σ-plane, the real axis of the t-plane between the points B and F being transformed to a circle, with centre at the origin and radius r_0, i.e.

$$t = i\left(\sigma - \frac{r_0^2}{\sigma}\right). \tag{75}$$

In order to use Sack's results, we require the coefficients in the expansion of ζ in terms of σ,

$$\zeta = f(\sigma) = \sigma + \sum_0^\infty \frac{a_n}{\sigma^n} \tag{76}$$

or

$$\frac{d\zeta}{d\sigma} = 1 - \sum_0^\infty \frac{n a_n}{\sigma^{n+1}}, \tag{77}$$

the latter form being more useful, since it avoids the expansion of the elliptic functions.

From equations (55) to (59), and (75), we have that

$$\frac{d\zeta}{d\sigma} = M\left(1 + \frac{ib_2}{\sigma} - \frac{r_0^2}{\sigma^2}\right)\left(1 + \frac{ia_2}{\sigma} - \frac{r_0^2}{\sigma^2}\right)^{1/2}\left(1 + \frac{ia_3}{\sigma} - \frac{r_0^2}{\sigma^2}\right)^{-1/2} \tag{78}$$

and, on comparing equations (77) and (78) we have the relations

$$M = 1 \qquad \text{and} \qquad b_2 = \tfrac{1}{2}(a_3 - a_2).$$

The former equation, with equations (64) and (67), gives that

$$\frac{2r_0}{s} = \lambda \frac{2K}{\pi} \frac{(1-\nu^2 k^2)^{1/2}}{(1-\nu^2)^{1/2}} \tag{79}$$

and the latter equation gives a check on the arithmetic, since it is satisfied by the algebraic expressions for b_2, a_2 and a_3.

In equation (78), we may write $b_2 = r_0 B_2$, $a_2 = r_0 A_2$ and $a_3 = r_0 A_3$, and then expand, by the multinomial theorem, in terms of $(r_0/\sigma)^n$, obtaining

$$\frac{d\zeta}{d\sigma} = 1 + \sum_0^\infty C_n \left(\frac{r_0}{\sigma}\right)^n$$

so that the a_n's of Sack's expansion are given by

$$a_n = -\frac{1}{n} C_{n+1} r_0^{n+1} \qquad \text{for} \qquad n > 0. \tag{80}$$

The coefficient a_0 is obtained by consideration of the co-ordinates of the point B, say, in the ζ and σ-planes. This results in

$$a_0 = -r_0\left\{i - \sum_1^\infty \frac{C_{n+1}}{n}(-i)^n\right\}$$

$$= r_0 C_0 \text{ say}. \tag{81}$$

The expression for l_v obtained by Sacks includes the infinite sum

$$\Sigma = \bar{a}_0 r_0^2 + \bar{a}_1 a_0 + \frac{\bar{a}_2 a_1}{r_0^2} + \ldots$$

$$= r_0^3\left\{\bar{C}_0 - \bar{C}_2 C_0 + \frac{\bar{C}_3 C_2}{2.1} + \ldots\right\}. \tag{82}$$

Thus

$$(l_v)_{\alpha=0} = \frac{4\pi}{Sb}\,\text{Imag.}\,\{\Sigma\}_{x=l}$$

$$= \frac{4\pi}{Sb}\left(\frac{K}{\pi}\right)^3\left[\frac{1-\nu^2k^2}{1-\nu^2}\right]^{3/2}\left(\frac{b}{2}\right)^3\lambda^3\,\text{Imag.}\,[\bar{C}_0 - \bar{C}_2C_0 + \ldots]$$

$$= \frac{\pi A}{2}\left(\frac{\lambda K}{\pi}\right)^3\left[\frac{1-\nu^2k^2}{1-\nu^2}\right]^{3/2}\text{Imag.}\,[\bar{C}_0 - \bar{C}_2C_0 + \ldots]. \tag{83}$$

The slope of the $l_v - \alpha$ curve is also affected by the drooped leading edges, and we have that

$$\frac{dl_v}{d\alpha} = -\frac{8\pi}{Sb}\,\text{Real}\int_0^l a_1 dx$$

$$= \frac{\pi}{3}\left(\frac{2K}{\pi}\right)^2\left(\frac{1-\nu^2k^2}{1-\nu^2}\right)\lambda^2\,\text{Real}\,(G_2)$$

$$= -\frac{\pi}{3}\left(\frac{2\lambda K}{\pi}\right)^2\left(\frac{1-\nu^2k^2}{1-\nu^2}\right)\left[1 - \frac{2k(1-\nu^2)}{(1-\nu^2k^2)}\{2\nu(1-k^2) + k(1-\nu^2)\}\right]. \tag{84}$$

The computation was carried out for $\lambda = 3/4$, with the coefficients a_n evaluated as far as a_8, with the result

$$l_v = 0{\cdot}025A - 0{\cdot}739\alpha. \tag{85}$$

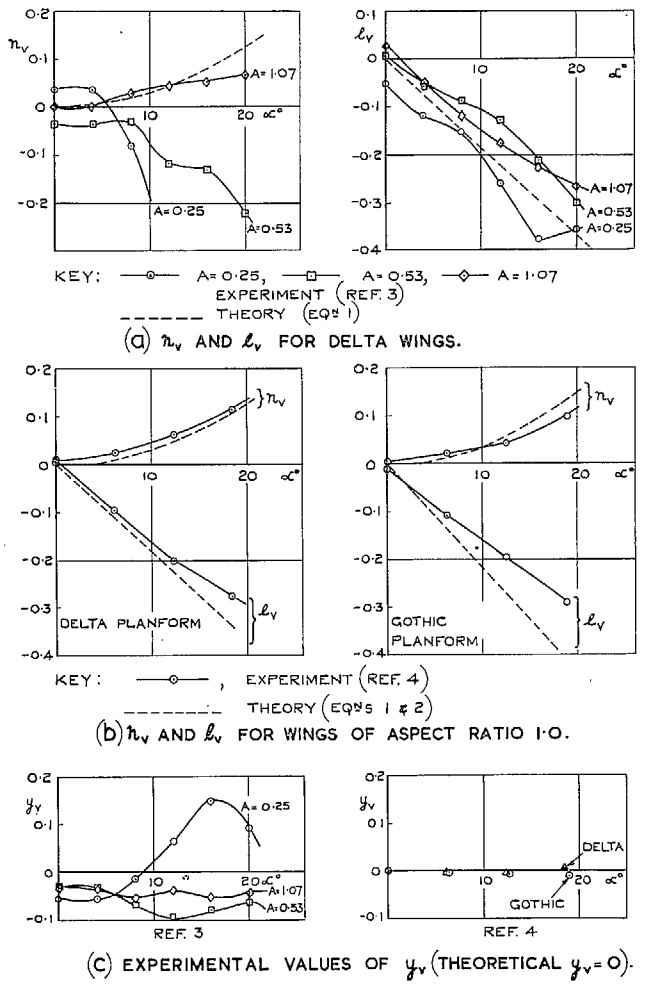

FIG. 1. Comparison between experiment and attached-flow theory for sideslip derivatives of flat-plate wings with no dihedral.

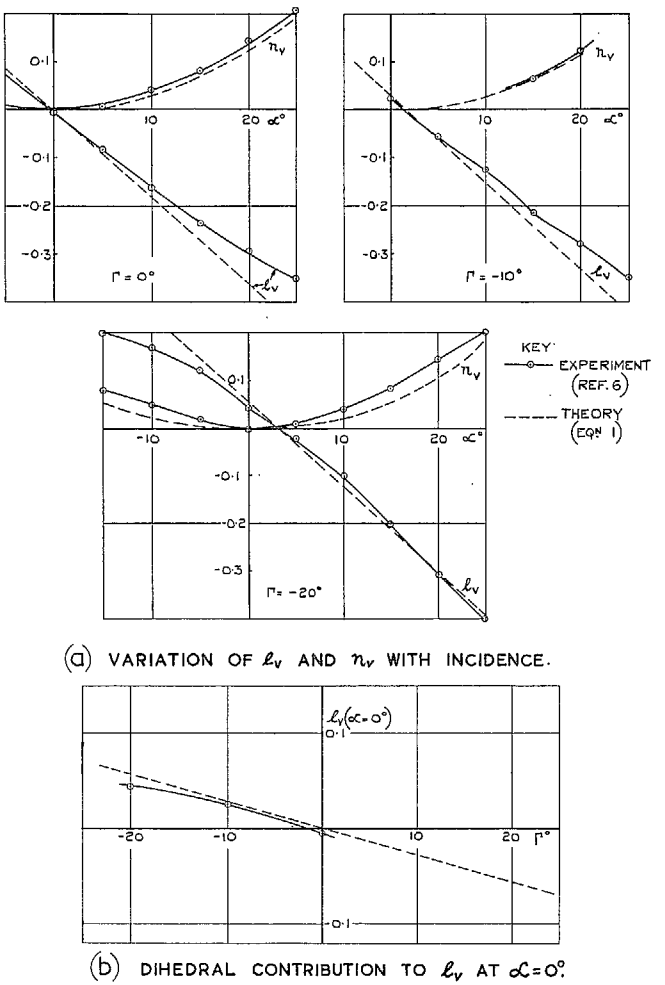

FIG. 2. Comparison between experiment and theory for l_v and n_v of a delta wing, aspect ratio = 1·0, with anhedral.

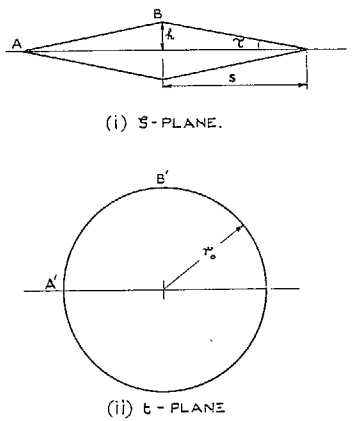

(a) WING WITH DIAMOND CROSS-SECTION. (PHYSICAL AND TRANSFORMATION PLANES)

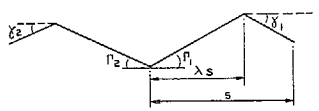

(b) WING WITH DIHEDRAL DISTRIBUTION.

FIG. 3. Spanwise sections of wings considered in Section 2.

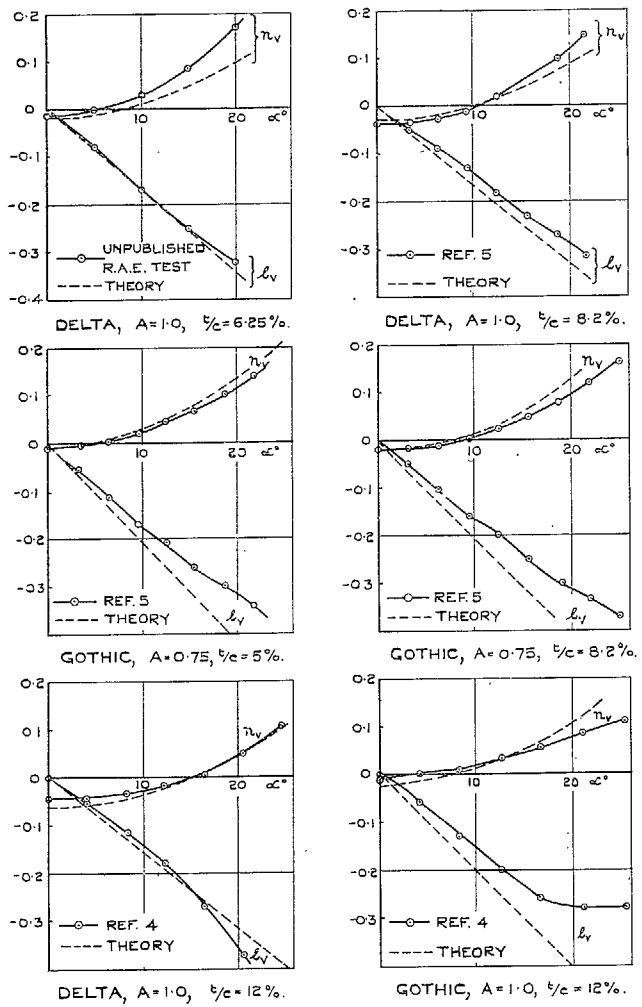

FIG. 4. Comparison between experiment and theory for l_v and n_v of wings with thickness.

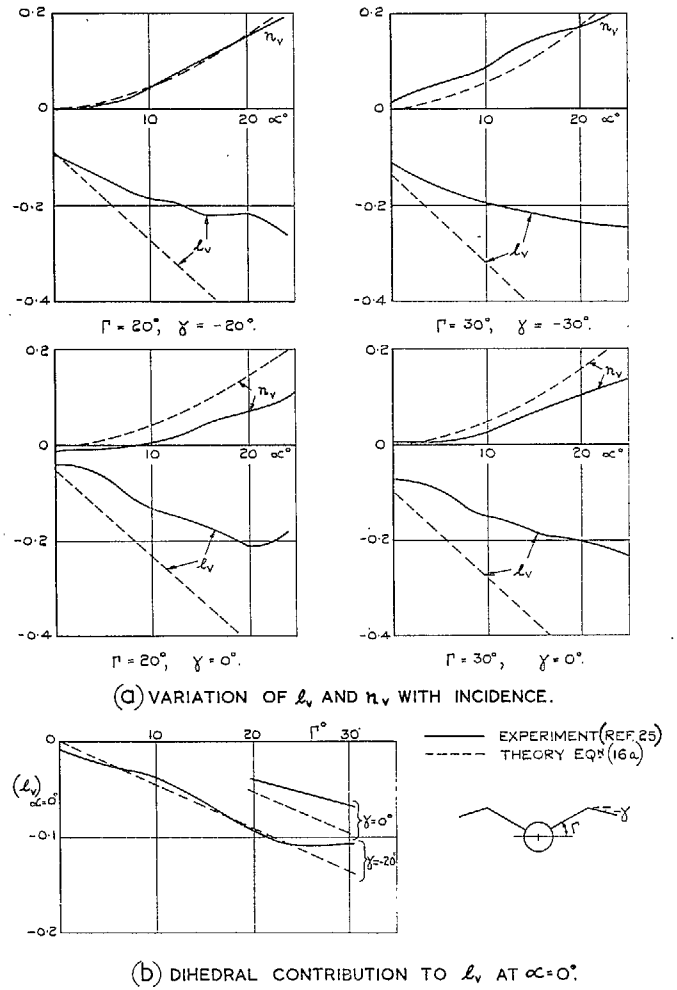

FIG. 5. Comparison between experiment and theory for l_v and n_v of a delta wing with part-span dihedral: $A = 1{\cdot}56$, $\lambda = 0{\cdot}667$.

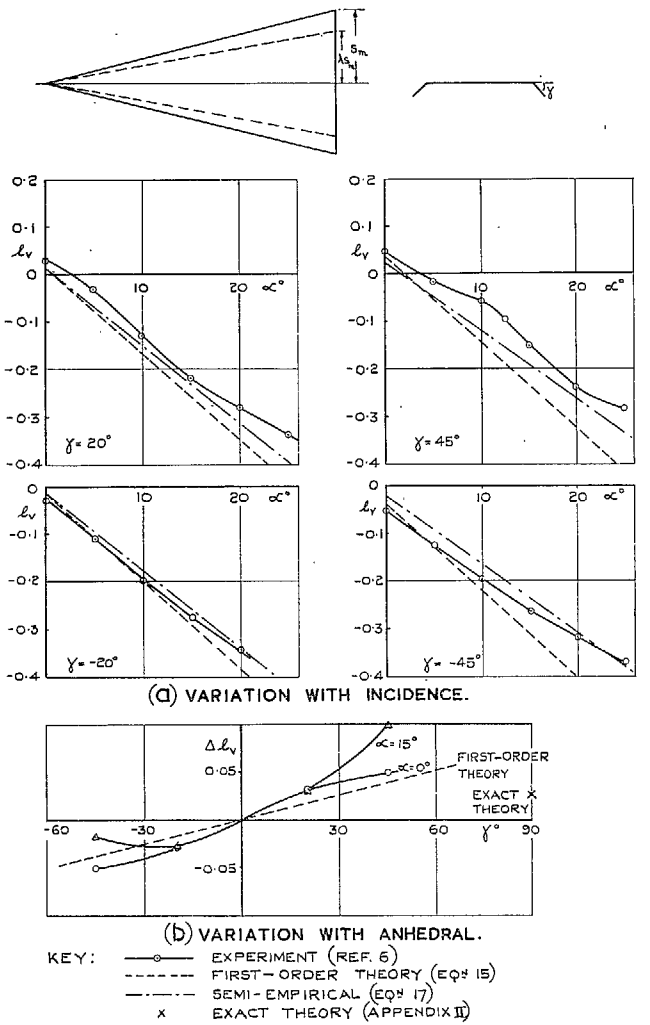

FIG. 6. Comparison between experiment and theory for l_v of a delta wing with drooped leading edges: $A = 1{\cdot}0$, $\lambda = 0{\cdot}75$.

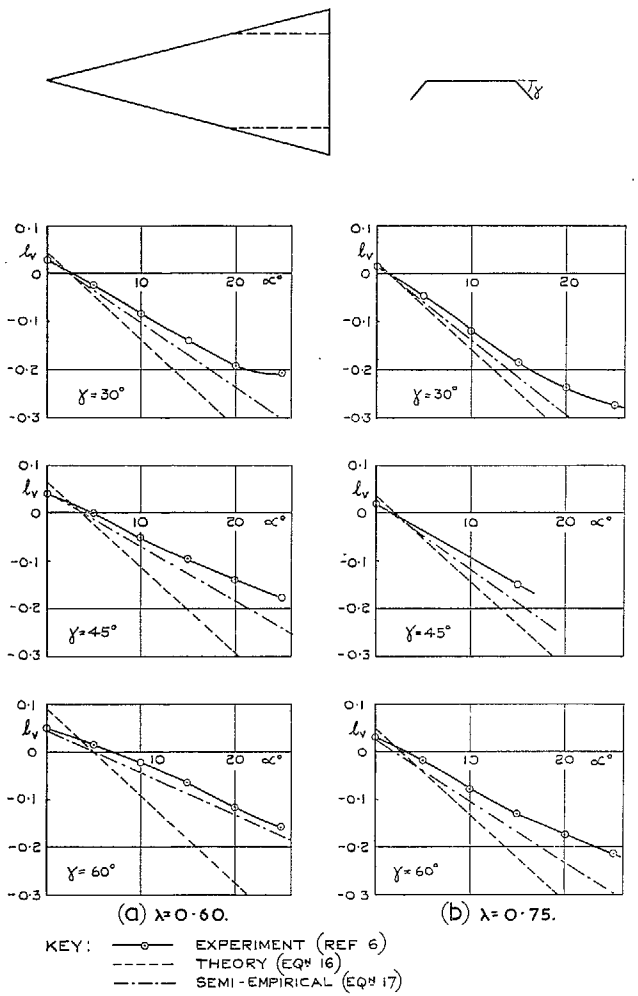

FIG. 7. Comparison between experiment and theory for l_v of a delta wing with drooped tips: $A = 1{\cdot}0$.

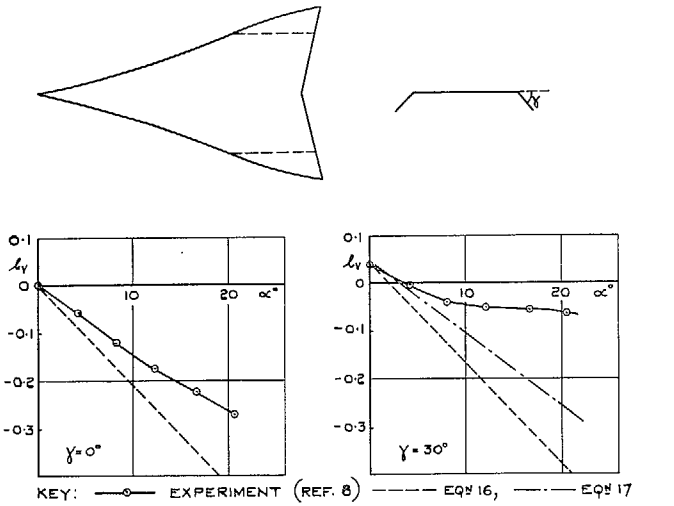

FIG. 8. Comparison between experiment and theory for l_v of an ogee wing with drooped tips: $A = 1{\cdot}31$, $\lambda = 0{\cdot}70$.

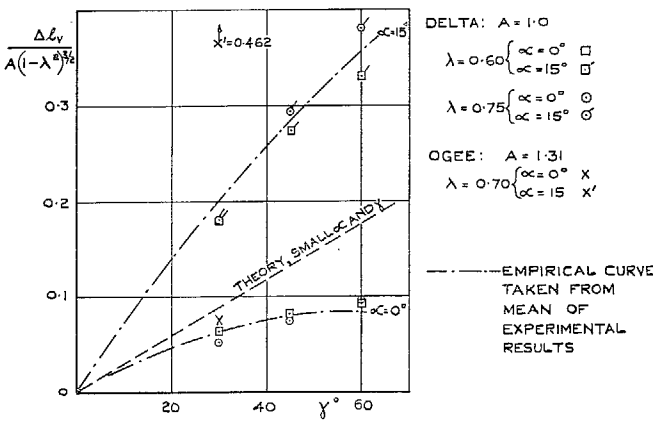

FIG. 9. Increment in l_v due to drooped tips on a delta and an ogee at $\alpha = 0°$ and $\alpha = 15°$.

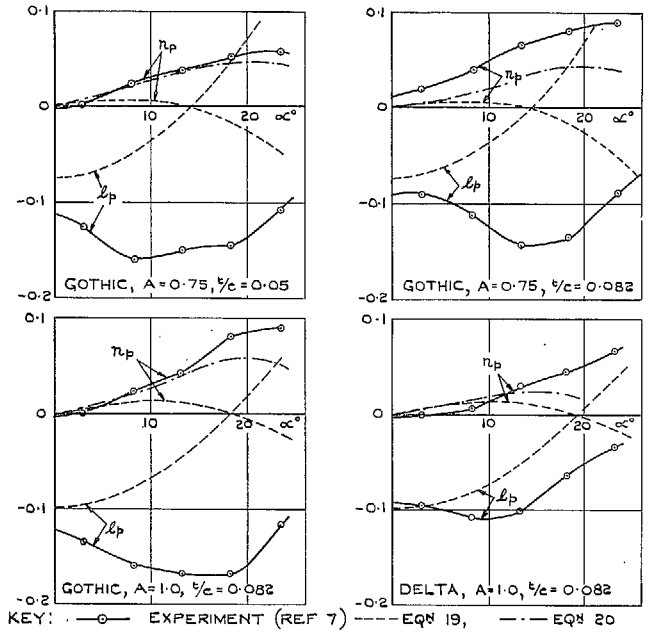

FIG. 10. Comparison between experiment and attached-flow theory for l_p and n_p of wings.

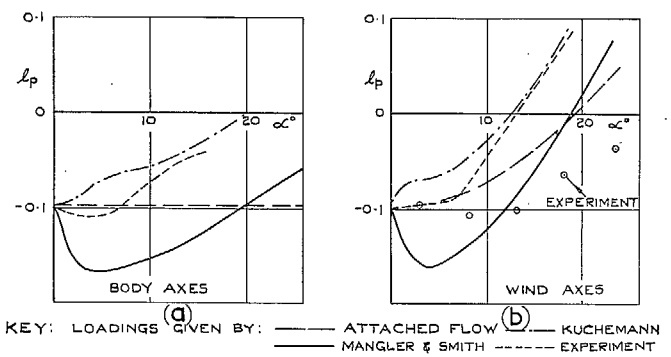

FIG. 11. Theoretical values of l_p in body and wind axes for a delta wing, $A = 1{\cdot}0$ with c.g. at $59{\cdot}3\%$ root chord.

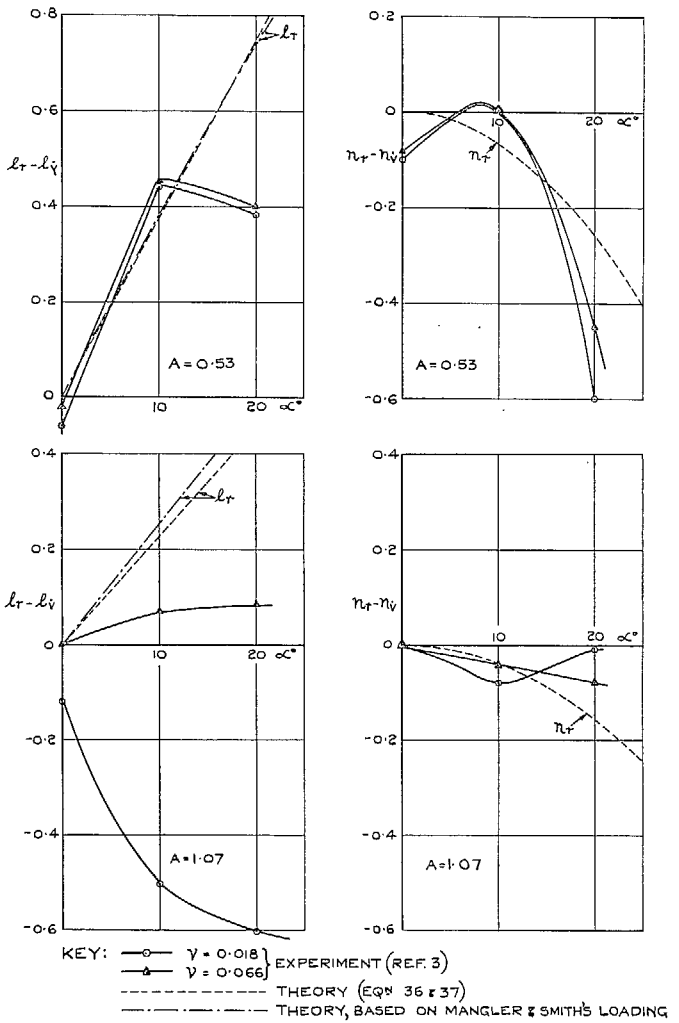

FIG. 12. Comparison between experiment and theory for l_r and n_r of delta wings.

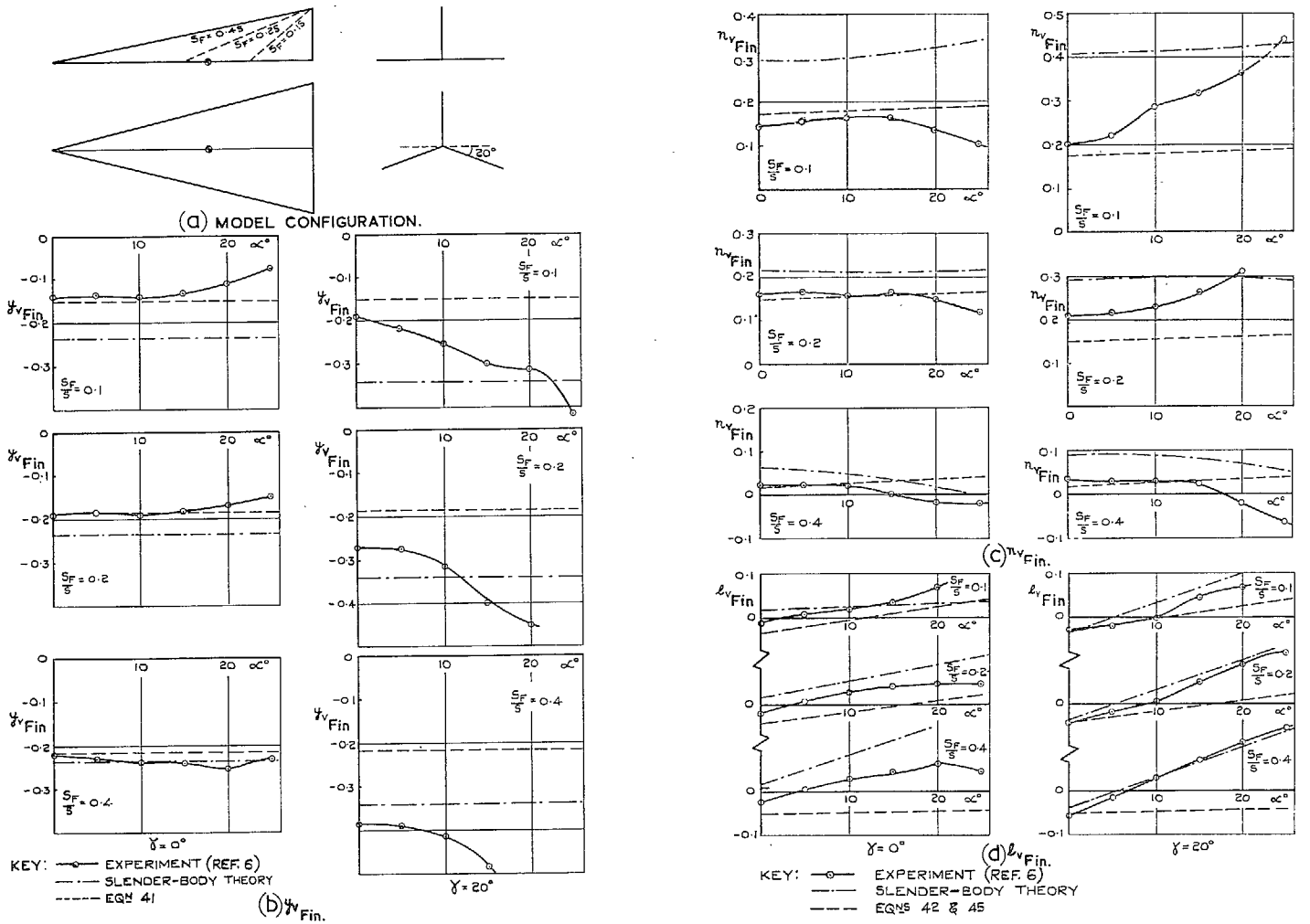

FIG. 13. Comparison between experiment, slender-body theory, and estimate from reflected fin, for fin contributions to y_v, l_v and n_v.

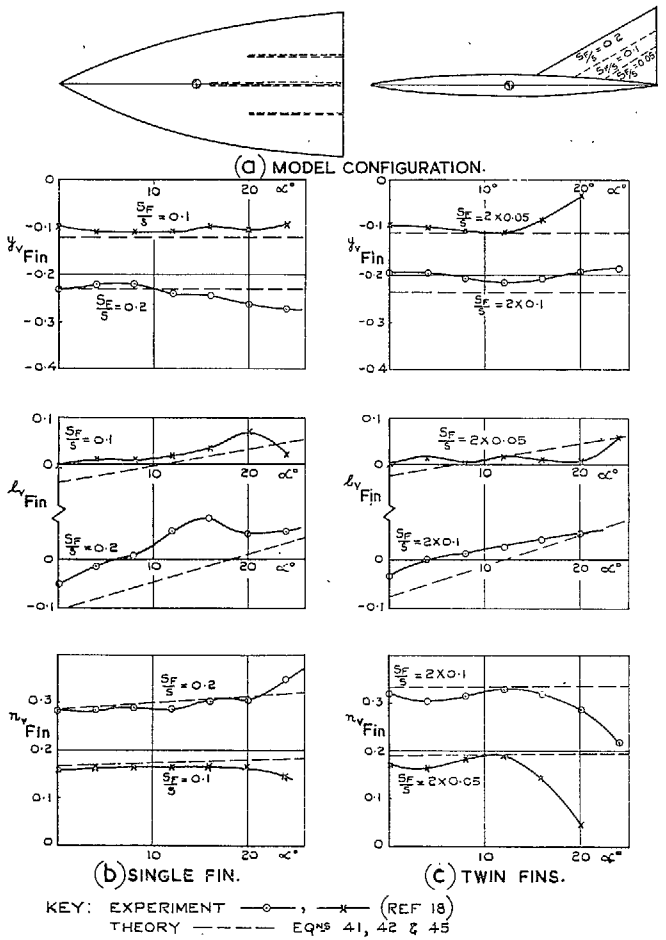

FIG. 14. Comparison between experiment and estimate from reflected fin for fin contributions to y_v, l_v and n_v.

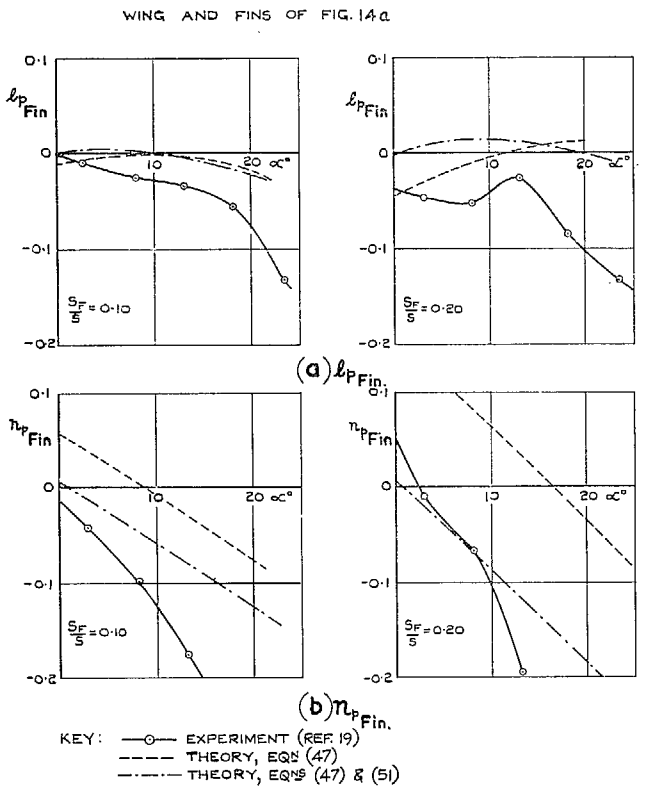

FIG. 15. Comparison between experiment and theory for fin contributions to l_p and n_p.

(91012) Wt. 66/2301 K.5 3/65 Hw.

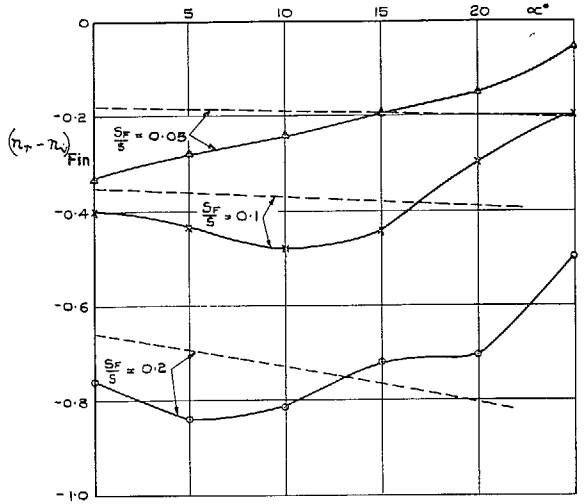

(a) WING & FINS OF FIG. 14a.

KEY: ——— BRISTOL EXPERIMENT (REF. 16), $\nu = 0.24$
– – – – – THEORY (EQN 54)

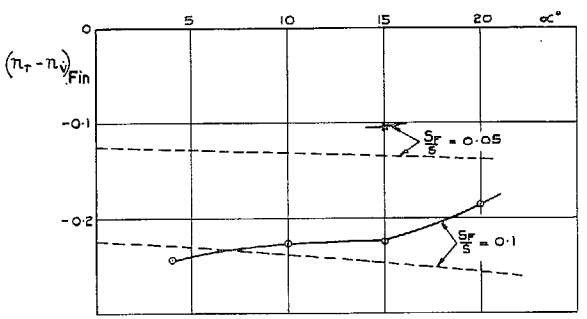

(b) TRIANGULAR FINS, 60° SWEEPBACK, ON ROUNDED DELTA.

KEY: ——— GRAY'S EXPERIMENT, $\nu = 0.25$ (UNPUBLISHED)
– – – – – THEORY (EQN 54)

FIG. 16. Comparison between experiment and theory for fin contributions to n_v–$n_{\dot{v}}$.

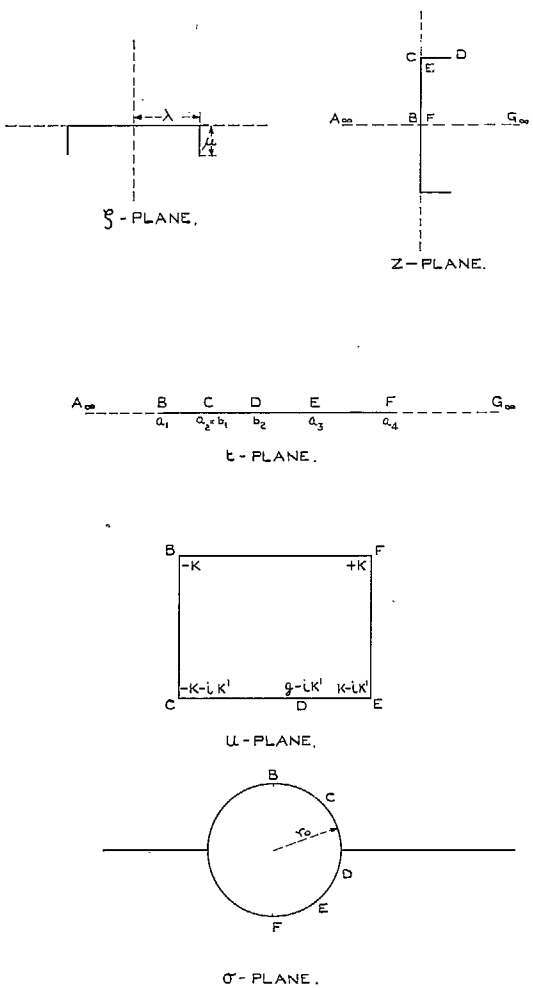

FIG. 17. Transformation planes used in Appendix II.

Publications of the Aeronautical Research Council

ANNUAL TECHNICAL REPORTS OF THE AERONAUTICAL RESEARCH COUNCIL (BOUND VOLUMES)

1942 Vol. I. Aero and Hydrodynamics, Aerofoils, Airscrews, Engines. 75*s.* (post 2*s.* 9*d.*)
Vol. II. Noise, Parachutes, Stability and Control, Structures, Vibration, Wind Tunnels. 47*s.* 6*d.* (post 2*s.* 3*d.*)

1943 Vol. I. Aerodynamics, Aerofoils, Airscrews. 80*s.* (post 2*s.* 6*d.*)
Vol. II. Engines, Flutter, Materials, Parachutes, Performance, Stability and Control, Structures. 90*s.* (post 2*s.* 9*d.*)

1944 Vol. I. Aero and Hydrodynamics, Aerofoils, Aircraft, Airscrews, Controls. 84*s.* (post 3*s.*)
Vol. II. Flutter and Vibration, Materials, Miscellaneous, Navigation, Parachutes, Performance, Plates and Panels, Stability, Structures, Test Equipment, Wind Tunnels. 84*s.* (post 3*s.*)

1945 Vol. I. Aero and Hydrodynamics, Aerofoils. 130*s.* (post 3*s.* 6*d.*)
Vol. II. Aircraft, Airscrews, Controls. 130*s.* (post 3*s.* 6*d.*)
Vol. III. Flutter and Vibration, Instruments, Miscellaneous, Parachutes, Plates and Panels, Propulsion. 130*s.* (post 3*s.* 3*d.*)
Vol. IV. Stability, Structures, Wind Tunnels, Wind Tunnel Technique. 130*s.* (post 3*s.* 3*d.*)

1946 Vol. I. Accidents, Aerodynamics, Aerofoils and Hydrofoils. 168*s.* (post 3*s.* 9*d.*)
Vol. II. Airscrews, Cabin Cooling, Chemical Hazards, Controls, Flames, Flutter, Helicopters, Instruments and Instrumentation, Interference, Jets, Miscellaneous, Parachutes. 168*s.* (post 3*s.* 3*d.*)
Vol. III. Performance, Propulsion, Seaplanes, Stability, Structures, Wind Tunnels. 168*s.* (post 3*s.* 6*d.*)

1947 Vol. I. Aerodynamics, Aerofoils, Aircraft. 168*s.* (post 3*s.* 9*d.*)
Vol. II. Airscrews and Rotors, Controls, Flutter, Materials, Miscellaneous, Parachutes, Propulsion, Seaplanes, Stability, Structures, Take-off and Landing. 168*s.* (post 3*s.* 9*d.*)

1948 Vol. I. Aerodynamics, Aerofoils, Aircraft, Airscrews, Controls, Flutter and Vibration, Helicopters, Instruments, Propulsion, Seaplane, Stability, Structures, Wind Tunnels. 130*s.* (post 3*s.* 3*d.*)
Vol. II. Aerodynamics, Aerofoils, Aircraft, Airscrews, Controls, Flutter and Vibration, Helicopters, Instruments, Propulsion, Seaplane, Stability, Structures, Wind Tunnels. 110*s.* (post 3*s.* 3*d.*)

Special Volumes

Vol. I. Aero and Hydrodynamics, Aerofoils, Controls, Flutter, Kites, Parachutes, Performance, Propulsion, Stability. 126*s.* (post 3*s.*)
Vol. II. Aero and Hydrodynamics, Aerofoils, Airscrews, Controls, Flutter, Materials, Miscellaneous, Parachutes, Propulsion, Stability, Structures. 147*s.* (post 3*s.*)
Vol. III. Aero and Hydrodynamics, Aerofoils, Airscrews, Controls, Flutter, Kites, Miscellaneous, Parachutes, Propulsion, Seaplanes, Stability, Structures, Test Equipment. 189*s.* (post 3*s.* 9*d.*)

Reviews of the Aeronautical Research Council

1939–48 3*s.* (post 6*d.*) 1949–54 5*s.* (post 5*d.*)

Index to all Reports and Memoranda published in the Annual Technical Reports

1909–1947 R. & M. 2600 (out of print)

Indexes to the Reports and Memoranda of the Aeronautical Research Council

Between Nos. 2351–2449	R. & M. No. 2450 2*s.* (post 3*d.*)
Between Nos. 2451–2549	R. & M. No. 2550 2*s.* 6*d.* (post 3*d.*)
Between Nos. 2551–2649	R. & M. No. 2650 2*s.* 6*d.* (post 3*d.*)
Between Nos. 2651–2749	R. & M. No. 2750 2*s.* 6*d.* (post 3*d.*)
Between Nos. 2751–2849	R. & M. No. 2850 2*s.* 6*d.* (post 3*d.*)
Between Nos. 2851–2949	R. & M. No. 2950 3*s.* (post 3*d.*)
Between Nos. 2951–3049	R. & M. No. 3050 3*s.* 6*d.* (post 3*d.*)
Between Nos. 3051–3149	R. & M. No. 3150 3*s.* 6*d.* (post 3*d.*)

HER MAJESTY'S STATIONERY OFFICE

from the addresses overleaf

Printed and published by
HER MAJESTY'S STATIONERY OFFICE

To be purchased from
York House, Kingsway, London W.C.2
423 Oxford Street, London W.1
13A Castle Street, Edinburgh 2
109 St. Mary Street, Cardiff
39 King Street, Manchester 2
50 Fairfax Street, Bristol 1
35 Smallbrook, Ringway, Birmingham 5
80 Chichester Street, Belfast 1
or through any bookseller

Printed in England

S.O. Code No. 23-3402